

Comprehensive analysis of fusion data well above the barrier

P. Eudes,^{1,*} Z. Basrak,^{2,†} F. Sébille,¹ V. de la Mota,¹ and G. Royer¹

¹SUBATECH, EMN-IN2P3/CNRS-Université de Nantes, Nantes, France

²Ruder Bošković Institute, Zagreb, Croatia

(Received 21 July 2014; published 12 September 2014)

We report on the comprehensive systematics of nearly 400 fusion-evaporation and/or fusion-fission cross-section data for a very large variety of systems over an energy range $\sim 3A$ to $155A$ MeV. Scaled by the reaction cross section and expressed as a function of the center-of-mass energy per nucleon, the fusion cross section displays a universal behavior. Within experimental errors, this behavior does not depend on system mass, mass asymmetry, or system isospin. The deduced homographic functional dependence for complete and summed complete and incomplete fusion excitation functions is derived from basic strong absorption model formulas for reaction cross sections and allows us to draw the main properties of these functions. The limiting energy for the complete fusion and the main characteristics (onset, maximum, and extinction) of the incomplete fusion excitation functions are determined. The complete fusion reaction process disappears around 6.5 MeV/nucleon and the incomplete one disappears at about 13 MeV/nucleon in the center-of-mass frame. The regularity in fusion data is particularly obvious for the evaporation-residue subset of the data ensemble. Adding the fusion-fission data component does not alter the general data trend but somewhat obscures it owing to the larger uncertainty and/or possible normalization problems.

DOI: 10.1103/PhysRevC.90.034609

PACS number(s): 25.70.Jj

I. INTRODUCTION

Displayed as a function of the inverse of center-of-mass energy, a fusion excitation function features three distinct regimes. They are generally referred to as regions I, II, and III. Region I opens at the reaction threshold, than steadily increases, and ends by the region II, corresponding to the saturation of fusion cross section, whereas in the region III the fusion process regularly diminishes. Using simple models such as the one of Bass [1], the evolution of each individual fusion excitation function can be described by three straight lines having a common functional form. At low energies, in regions I and II, an important amount of experimental data exists. Since the 1970s these data have been subjected to several systematics aimed at confronting specific theoretical models with the available data [1–11]. In these two regions only complete fusion (CF) takes place. Exception to this general trend are nuclear reactions involving weakly bound nuclei such as ^6Li or ^9Be or unstable nuclei that can quite easily release a few valence nucleons before the core nucleus fuses with the target (for a review on the subject see, e.g., Refs. [12,13]).

In region III the reaction mechanism is significantly modified. Indeed, with increasing incident energy the so-called pre-equilibrium emission sets in, rendering the compound nucleus less massive than the whole reaction system and giving rise to an incomplete fusion (IF) process. In the fusion region III two competing fusion mechanisms exist and, accordingly, two distinct fusion excitation functions are measured: one corresponding to the CF reaction mechanism, which decreases steadily, and another one corresponding to the sum of the CF and IF cross sections, which decreases as well, although the

IF component starts by increasing. Total fusion reaction cross section steadily decreases. These phenomena were studied in the 1970s and 1980s, while very few fusion studies in the fusion region III have been reported in the past 15 years (the current interest being focused on the fusion phenomena around and below the Coulomb barrier [13]). To the best of our knowledge, the systematic and comparative study of the relatively limited fusion data set in region III has been carried out in two works only [14,15]. In the first one, Morgenstern *et al.* in 1984 [14] have studied the evolution of the ratio between CF and IF + CF as a function of incident velocity of the lighter partner. The authors have concluded that the mass asymmetry has a strong influence on the onset of incomplete fusion and on the limiting energy of complete fusion. The second systematics has been published by the INDRA Collaboration in 2006 [15], reporting a fusion excitation function relative to 35 fusion cross sections belonging to 7 light and almost symmetric systems.

In this paper we present a coherent analysis of experimental fusion cross sections σ_{fus} for both complete and incomplete fusion components arising from the evaporation residue or from the fusion-fission processes limited to energies higher than about $3A - 4A$ MeV. Other possible reaction mechanisms which may proceed by a compound nucleus formation and, thus, by fusion (like ternary fission or multifragmentation) are not our concern because of the lacking cross-section data. In this work we are concerned with a unified description of fusion data as a function of energy. Accordingly, we willingly excluded from our analysis those reaction systems which are known by their exclusive and peculiar behavior, i.e., displaying oscillatory or an otherwise structured fusion excitation function. That is the case of many light reaction systems and especially of those reputed to form *nuclear molecules*, among which the $^{12}\text{C} + ^{12}\text{C}$, $^{12}\text{C} + ^{16}\text{O}$, and $^{16}\text{O} + ^{16}\text{O}$ systems are known to display the strongly structured (oscillatory) fusion excitation functions (for a review on the fusion between the

*eudes@subatech.in2p3.fr

†basrak@irb.hr

p -shell nuclei, see, e.g., Refs. [16–18]). As discussed above, fusion reactions involving exotic and weakly bound nuclei proceed through a breakup mechanism. Thus, they bypass the compound-nucleus formation of the whole system already at the reaction threshold. Consequently, these reaction cases are beyond the scope of the present work.

Preliminary results of this work have been reported earlier [19,20]. In a recent letter [21] we have presented the subset of fusion-evaporation cross sections relative to those works claiming that the fusion-fission component either does not exist or is negligible. The letter also reports on a rather favorable comparison of these experimental fusion data with a semiclassical transport model prediction of the fusion excitation function [21,22].

II. THE SYSTEMATICS

A scrutiny scan of the published fusion data at incident energy higher than about $3A - 4A$ MeV over the past 40 years ended with 382 CF and CF + IF σ_{fus} values belonging to 81 different reaction systems. The full set of σ_{fus} data is reviewed in Table I. From top to bottom the yields are ordered by increasing values of the system mass $A_{\text{tot}} = A_t + A_p$, with A_p (A_t) being projectile (target) mass. For a given A_{tot} value, the data are sorted by increasing projectile mass, and for

each A_p value by increasing incident energy per nucleon $E_{\text{in}} = E_{\text{lab}}/\text{nucleon}$ and by referenced works.

Figure 1 displays all 346 collected fusion data listed in the column 5 of Table I as a function of incident energy E_{in} (given in column 3 of Table I). The systems are sorted out by increasing mass A_{tot} and differentiated by varied symbols and a color code (online only): blue, cyan, and green symbols label the lighter systems ($A_{\text{tot}} \lesssim 100$); pink, red, and orange symbols label the heavier ones ($100 \lesssim A_{\text{tot}} \lesssim 200$), while the heaviest systems are dark red. The same symbol and color code are used for a given system throughout this paper.

The span in the total system mass A_{tot} ranges between 26 and 278, the system mass asymmetry $\mu = |A_t - A_p|/(A_t + A_p)$ from 0 to 0.886, the neutron to proton ratio $N_{\text{tot}}/Z_{\text{tot}}$ from 1 to 1.536, while the incident energy lies between $3A$ and $155A$ MeV. A mere glance at Fig. 1 reveals a stack of fusion data below about $10A$ MeV. Although this domain of the σ_{fus} vs E_{in} plane is dominated by heavier systems (red-orange-dark-red symbols), the stack of lighter systems (blue-cyan-green symbols) around $\sigma_{\text{fus}} \approx 1$ b is very strongly present. Energies above about $20A$ MeV are barely covered by the data. A more complete information on the ensemble of data may be inferred from Fig. 2, which displays the frequency of available σ_{fus} as a function of A_{tot} [Fig. 2(a)], μ [Fig. 2(b)], system $N_{\text{tot}}/Z_{\text{tot}}$ ratio [Fig. 2(c)], and E_{in} [Fig. 2(d)]. A correlation between A_{tot} and μ is also plotted [Fig. 2(e)]. It shows an (expected) absence

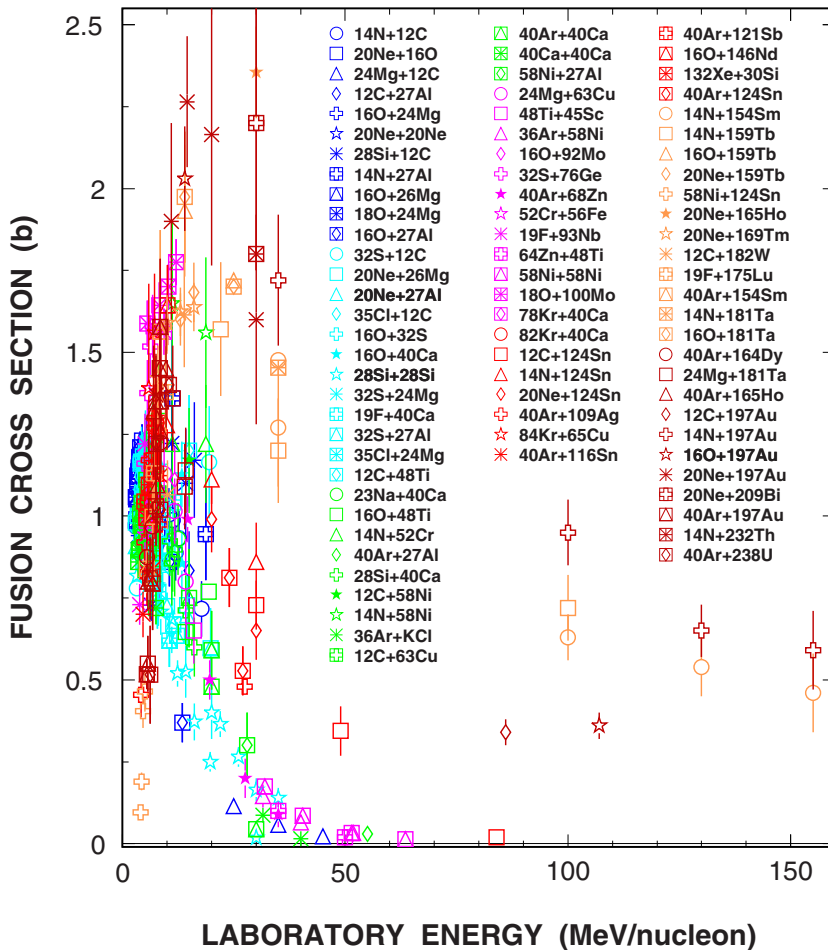


FIG. 1. (Color online) Raw fusion cross sections σ_{fus} plotted as a function of incident energy per nucleon in the laboratory reference frame $E_{\text{lab}}/\text{nucleon} = E_{\text{in}}$. The inventoried systems are distinguished among them by symbols and levels of gray (a color code online). The same symbols and the levels of gray (color code) are used throughout this paper. References to all σ_{fus} data are given in Table I.

TABLE I. Experimentally deduced fusion cross sections σ_{fus} published in the literature so far. In the case when both the complete and incomplete fusion cross sections have been reported from the same measurement the complete fusion contribution is stated in the column CF. For each entry, the reference to original work, the incident energy per nucleon E_{in} , the corresponding center-of-mass energy per nucleon $E_{\text{c.m.}}/A_{\text{tot}}$, σ_{fus} , CF, and the σ_{fus} normalized by the phenomenological reaction cross section σ_{reac}^T of Tripathi [24] are given.

System	Ref.	E_{in} (MeV/nucleon)	$E_{\text{c.m.}}/A_{\text{tot}}$ (MeV/nucleon)	σ_{fus} (mb)	CF (mb)	$\sigma_{\text{fus}}/\sigma_{\text{reac}}^T$
$^{14}\text{N} + ^{12}\text{C}$	[25]	3.14	0.78	967 \pm 75		0.780 \pm 0.061
		3.80	0.94	964 \pm 75		0.723 \pm 0.056
		4.29	1.07	932 \pm 75		0.675 \pm 0.054
		6.16	1.53	895 \pm 80		0.604 \pm 0.054
		7.59	1.89	913 \pm 80		0.604 \pm 0.053
		10.39	2.58	1005 \pm 80		0.658 \pm 0.052
		11.94	2.97	888 \pm 85		0.583 \pm 0.056
		12.72	3.16	932 \pm 85		0.614 \pm 0.056
	[26]	11.29	2.81	987 \pm 80		0.647 \pm 0.052
		17.71	4.40	717 \pm 85		0.486 \pm 0.058
$^{20}\text{Ne} + ^{16}\text{O}$	[27]	3.40	0.84	1119 \pm 110		0.805 \pm 0.079
		5.74	1.42	1117 \pm 110		0.654 \pm 0.064
		6.10	1.51	1040 \pm 110		0.601 \pm 0.064
		6.85	1.69	1144 \pm 100		0.646 \pm 0.056
		7.80	1.93	936 \pm 90		0.518 \pm 0.050
$^{24}\text{Mg} + ^{12}\text{C}$	[28]	25.00	5.56	125 \pm 20		0.074 \pm 0.012
		35.00	7.78	58		0.036
		45.00	10.00	22		0.015
$^{12}\text{C} + ^{27}\text{Al}$	[29]	5.32	1.13	1140 \pm 160		0.692 \pm 0.097
		6.75	1.44	1150 \pm 160		0.658 \pm 0.092
		7.14	1.52	1110 \pm 155		0.629 \pm 0.088
		8.04	1.71	1000 \pm 150		0.557 \pm 0.084
		8.13	1.73	854 \pm 120		0.475 \pm 0.067
		15.00	3.20	834 \pm 120		0.454 \pm 0.065
$^{16}\text{O} + ^{24}\text{Mg}$	[30]	3.00	0.72	972 \pm 39		0.784 \pm 0.031
		3.25	0.78	1037 \pm 62		0.782 \pm 0.047
		3.50	0.84	1036 \pm 41		0.741 \pm 0.029
		3.81	0.91	1070 \pm 43		0.726 \pm 0.029
		4.13	0.99	1074 \pm 65		0.698 \pm 0.042
		4.50	1.08	1101 \pm 44		0.687 \pm 0.027
		5.06	1.22	1116 \pm 45		0.665 \pm 0.027
$^{20}\text{Ne} + ^{20}\text{Ne}$	[27]	3.40	0.85	1079 \pm 95		0.756 \pm 0.067
		5.85	1.46	1140 \pm 95		0.630 \pm 0.052
		6.30	1.58	1113 \pm 90		0.603 \pm 0.049
		7.00	1.75	1111 \pm 100		0.589 \pm 0.053
		7.80	1.95	1080 \pm 60		0.562 \pm 0.031
$^{28}\text{Si} + ^{12}\text{C}$	[31]	3.57	0.75	940 \pm 86		0.699 \pm 0.064
		4.46	0.94	1040 \pm 96		0.684 \pm 0.063
		5.36	1.13	1185 \pm 86		0.727 \pm 0.053
		6.36	1.34	1150 \pm 81		0.672 \pm 0.047
		11.04	2.32	1222 \pm 183	772 \pm 131	0.663 \pm 0.099
		14.18	2.98	1100 \pm 165	597 \pm 101	0.596 \pm 0.089
	[32]	16.14	3.39	1171 \pm 176	537 \pm 91	0.637 \pm 0.096
		5.71	1.20	844 \pm 55		0.507 \pm 0.033
		6.43	1.35	728 \pm 48		0.424 \pm 0.028
		11.21	2.52	1360 \pm 200		0.709 \pm 0.104
$^{14}\text{N} + ^{27}\text{Al}$	[33]	18.71	4.21	945 \pm 140		0.500 \pm 0.074
		3.11	0.73	1052 \pm 63		0.774 \pm 0.046
$^{16}\text{O} + ^{26}\text{Mg}$	[30]	3.36	0.79	1124 \pm 67		0.782 \pm 0.047
		3.67	0.87	1148 \pm 69		0.755 \pm 0.045
		3.85	0.91	1181 \pm 47		0.756 \pm 0.030
		4.04	0.95	1177 \pm 71		0.735 \pm 0.044

TABLE I. (*Continued.*)

System	Ref.	E_{in} (MeV/nucleon)	$E_{\text{c.m.}}/A_{\text{tot}}$ (MeV/nucleon)	σ_{fus} (mb)	CF (mb)	$\sigma_{\text{fus}}/\sigma_{\text{reac}}^T$
$^{18}\text{O} + ^{24}\text{Mg}$	[30]	4.49	1.06	1196 ± 48		0.712 ± 0.029
		5.06	1.19	1177 ± 50		0.670 ± 0.028
		3.05	0.75	1058 ± 63		0.755 ± 0.045
		3.33	0.82	1090 ± 65		0.732 ± 0.044
		3.50	0.86	1137 ± 45		0.741 ± 0.029
		3.72	0.91	1179 ± 71		0.743 ± 0.045
		4.00	0.98	1210 ± 48		0.736 ± 0.029
$^{16}\text{O} + ^{27}\text{Al}$	[34]	3.13	0.73	990 ± 50		0.763 ± 0.039
		3.75	0.88	1135 ± 50		0.764 ± 0.034
		4.06	0.95	1185 ± 50		0.761 ± 0.032
		4.38	1.02	1230 ± 50		0.760 ± 0.031
		4.69	1.10	1185 ± 50		0.710 ± 0.030
	[35]	5.00	1.17	1160 ± 50		0.677 ± 0.029
		5.06	1.18	1020 ± 115		0.592 ± 0.067
		6.56	1.53	1040 ± 60		0.559 ± 0.032
		7.88	1.84	960 ± 70		0.498 ± 0.036
		10.50	2.45	860 ± 75		0.432 ± 0.038
$^{32}\text{S} + ^{12}\text{C}$	[36]	13.44	3.14	370 ± 60	274 ± 60	0.185 ± 0.030
		3.21	0.63	780 ± 13		0.646 ± 0.011
		3.40	0.67	1006 ± 50		0.789 ± 0.039
	[37]	4.10	0.81	1171 ± 60		0.804 ± 0.041
		4.53	0.90	1123 ± 40		0.730 ± 0.026
		5.00	0.99	1166 ± 75		0.725 ± 0.047
		19.50	3.87	1165 ± 171	505 ± 82	0.616 ± 0.090
$^{20}\text{Ne} + ^{26}\text{Mg}$	[42]	3.00	0.74	980 ± 67		0.729 ± 0.050
		4.20	1.03	1166 ± 80		0.685 ± 0.047
		4.65	1.14	1182 ± 75		0.662 ± 0.042
		5.25	1.29	1198 ± 70		0.640 ± 0.037
		6.00	1.47	1163 ± 75		0.596 ± 0.038
		7.50	1.84	1046 ± 75	828 ± 85	0.509 ± 0.037
		10.10	2.48	910 ± 65	582 ± 75	0.426 ± 0.030
		14.50	3.56	728 ± 90	365 ± 50	0.337 ± 0.042
		19.75	4.85	596 ± 95	216 ± 40	0.280 ± 0.045
		3.00	0.73	908 ± 70		0.717 ± 0.055
$^{20}\text{Ne} + ^{27}\text{Al}$	[43]	4.05	0.99	1172 ± 65		0.725 ± 0.040
		4.25	1.04	1178 ± 95		0.708 ± 0.057
		4.65	1.14	1165 ± 70		0.668 ± 0.040
		5.25	1.28	1185 ± 72		0.645 ± 0.039
		6.00	1.47	1115 ± 70		0.580 ± 0.036
		7.50	1.83	988 ± 80	936 ± 70	0.486 ± 0.039
		9.00	2.20	852 ± 85	758 ± 80	0.406 ± 0.041
		14.50	3.54	698 ± 105	403 ± 100	0.323 ± 0.049
		19.75	4.83	600 ± 120	235 ± 95	0.281 ± 0.056
		6.90	1.69	1170 ± 30		0.586 ± 0.015
		10.50	2.57	940 ± 60		0.441 ± 0.028
$^{35}\text{Cl} + ^{12}\text{C}$	[44]	3.57	0.68	1001 ± 170	970 ± 160	0.743 ± 0.126
		4.00	0.76	1066 ± 167	1013 ± 156	0.729 ± 0.114
		4.40	0.84	1084 ± 167	1036 ± 155	0.700 ± 0.108
	[45]	5.14	0.98	1081 ± 242		0.648 ± 0.145
		5.71	1.09	982 ± 143		0.566 ± 0.082
$^{16}\text{O} + ^{32}\text{S}$	[46]	7.94	1.51	788 ± 105		0.417 ± 0.056
		10.50	2.33	620 ± 80		0.301 ± 0.039
$^{16}\text{O} + ^{40}\text{Ca}$	[47]	3.11	0.63	884 ± 35		0.829 ± 0.033
		3.47	0.71	974 ± 50		0.782 ± 0.040
		3.92	0.80	1182 ± 65		0.834 ± 0.046

TABLE I. (*Continued.*)

System	Ref.	E_{in} (MeV/nucleon)	$E_{\text{c.m.}}/A_{\text{tot}}$ (MeV/nucleon)	σ_{fus} (mb)	CF (mb)	$\sigma_{\text{fus}}/\sigma_{\text{reac}}^T$
$^{28}\text{Si} + ^{28}\text{Si}$	[48]	4.65	0.95	1172 ± 53		0.721 ± 0.033
		6.47	1.32	1179 ± 55		0.613 ± 0.029
		8.73	1.78	1153 ± 100		0.551 ± 0.048
		13.38	2.73	1127 ± 100		0.510 ± 0.045
		13.38	2.73	856 ± 100	528 ± 100	0.387 ± 0.045
	[49]	3.21	0.80	817 ± 26		0.691 ± 0.022
		3.57	0.89	946 ± 35		0.696 ± 0.026
		3.93	0.98	1003 ± 40		0.668 ± 0.027
		4.29	1.07	1040 ± 32		0.642 ± 0.020
		5.00	1.25	1067 ± 35		0.593 ± 0.019
$^{28}\text{Si} + ^{28}\text{Si}$	[50]	6.21	1.55	852 ± 85		0.426 ± 0.042
		7.68	1.92	788 ± 78		0.367 ± 0.036
		8.57	2.14	708 ± 70		0.321 ± 0.032
		11.04	2.76	685 ± 103	470 ± 94	0.298 ± 0.045
		14.18	3.55	525 ± 79	326 ± 65	0.224 ± 0.034
	[51]	16.14	4.03	372 ± 56	229 ± 46	0.159 ± 0.024
		12.40	3.10	520 ± 40		0.224 ± 0.017
		19.70	4.93	250 ± 30		0.107 ± 0.013
		30.00	7.50	18 ± 4		0.008 ± 0.002
		20.00	5.00	400 ± 80		0.172 ± 0.034
$^{32}\text{S} + ^{24}\text{Mg}$	[52]	22.00	5.50	365 ± 40		0.157 ± 0.017
		26.00	6.50	265 ± 30		0.116 ± 0.013
		30.00	7.50	165 ± 35		0.074 ± 0.016
		35.00	8.75	140 ± 30		0.064 ± 0.014
		3.95	0.97	1060 ± 80		0.698 ± 0.053
	[53]	4.40	1.08	1075 ± 55		0.648 ± 0.033
		5.00	1.22	1075 ± 75		0.595 ± 0.042
		5.75	1.41	1170 ± 120		0.603 ± 0.062
		6.25	1.53	1050 ± 110		0.522 ± 0.055
		6.06	1.48	1005 ± 65		0.506 ± 0.033
$^{19}\text{F} + ^{40}\text{Ca}$	[55]	7.47	1.83	900 ± 70	855 ± 70	0.422 ± 0.033
		8.69	2.13	845 ± 95	790 ± 90	0.381 ± 0.043
		3.45	0.75	1000 ± 25		0.744 ± 0.019
		4.13	0.90	1160 ± 25		0.723 ± 0.016
		5.03	1.10	1137 ± 22		0.620 ± 0.012
	[57]	5.42	1.18	1085 ± 20		0.569 ± 0.010
		6.00	1.31	1111 ± 25		0.556 ± 0.013
		9.00	1.96	1018 ± 48	764 ± 40	0.453 ± 0.021
		11.37	2.48	1042 ± 48	626 ± 40	0.448 ± 0.021
$^{32}\text{S} + ^{27}\text{Al}$	[56]	4.43	1.10	1070 ± 20		0.627 ± 0.012
		4.77	1.18	1065 ± 20		0.592 ± 0.011
		5.47	1.36	1045 ± 25		0.537 ± 0.013
		5.86	1.45	975 ± 25		0.485 ± 0.012
		7.09	1.76	864 ± 25		0.399 ± 0.012
	[35]	7.94	1.97	862 ± 35	830 ± 35	0.386 ± 0.016
		10.00	2.48	726 ± 40	660 ± 45	0.310 ± 0.017
		11.44	2.84	670 ± 40	580 ± 50	0.281 ± 0.017
		12.28	3.05	635 ± 40	465 ± 45	0.265 ± 0.017
		10.50	2.61	620 ± 80		0.263 ± 0.034
$^{35}\text{Cl} + ^{24}\text{Mg}$	[58]	7.86	1.90	859 ± 203		0.385 ± 0.088
	[59]	8.07	1.95	770 ± 105	600 ± 105	0.343 ± 0.047
$^{12}\text{C} + ^{48}\text{Ti}$	[29]	6.75	1.08	943 ± 130		0.489 ± 0.067
		8.13	1.30	938 ± 130		0.462 ± 0.064
		15.00	2.40	1200 ± 170		0.552 ± 0.078

TABLE I. (*Continued.*)

System	Ref.	E_{in} (MeV/nucleon)	$E_{\text{c.m.}}/A_{\text{tot}}$ (MeV/nucleon)	σ_{fus} (mb)	CF (mb)	$\sigma_{\text{fus}}/\sigma_{\text{reac}}^T$
$^{23}\text{Na} + ^{40}\text{Ca}$	[57]	11.30	2.62	869 ± 100	574 ± 75	0.358 ± 0.041
		12.48	2.89	930 ± 110	512 ± 85	0.380 ± 0.045
$^{16}\text{O} + ^{\text{nat}}\text{Ti}$	[60]	14.19	2.66	647		0.274
		19.38	3.63	770		0.326
$^{14}\text{N} + ^{52}\text{Cr}$	[33]	11.21	1.87	1220 ± 180		0.541 ± 0.080
		18.71	3.13	1220 ± 180		0.530 ± 0.078
$^{40}\text{Ar} + ^{27}\text{Al}$	[61]	55.00	13.23	<30		0.013
$^{28}\text{Si} + ^{40}\text{Ca}$	[57]	10.64	2.58	923 ± 106	646 ± 100	0.372 ± 0.043
		11.68	2.83	898 ± 143	548 ± 130	0.356 ± 0.057
	[62]	11.04	2.67	855 ± 128	631 ± 126	0.342 ± 0.051
		14.18	3.43	712 ± 107	519 ± 104	0.277 ± 0.042
$^{12}\text{C} + ^{58}\text{Ni}$	[29]	16.14	3.91	600 ± 90	379 ± 76	0.232 ± 0.035
		5.32	0.76	956 ± 130		0.584 ± 0.079
		6.75	0.96	1217 ± 170		0.648 ± 0.090
		8.04	1.14	1050 ± 150		0.522 ± 0.075
		8.13	1.15	1240 ± 175		0.614 ± 0.087
$^{14}\text{N} + ^{58}\text{Ni}$	[33]	15.00	2.13	1170 ± 160		0.522 ± 0.071
		11.21	1.76	1650 ± 250		0.729 ± 0.110
$^{36}\text{Ar} + \text{KCl}$	[63]	18.71	2.93	1560 ± 230		0.664 ± 0.098
		31.58	7.89	87 ± 10		0.033 ± 0.004
		40.03	10.01	15 ± 10		0.006 ± 0.004
$^{12}\text{C} + ^{63}\text{Cu}$	[29]	51.78	12.94	4		0.002
		5.32	0.72	1110 ± 150		0.658 ± 0.089
		6.75	0.91	886 ± 120		0.457 ± 0.062
		8.04	1.08	1070 ± 150		0.515 ± 0.072
$^{40}\text{Ar} + ^{40}\text{Ca}$	[64]	8.13	1.09	1290 ± 175		0.618 ± 0.084
		4.02	1.00	1008 ± 82		0.641 ± 0.052
		4.75	1.19	1005 ± 81		0.530 ± 0.043
		5.90	1.48	897 ± 61		0.402 ± 0.027
	[52]	6.83	1.71	824 ± 56		0.342 ± 0.023
		15.00	3.75	750 ± 150		0.259 ± 0.052
		20.00	5.00	480		0.165
		20.00	5.00	590 ± 120		0.203 ± 0.041
$^{40}\text{Ca} + ^{40}\text{Ca}$	[68]	[67]	30.00	7.50	45 ± 20	0.016 ± 0.007
		3.55	0.89	860 ± 50		0.846 ± 0.049
		3.67	0.92	895 ± 50		0.808 ± 0.045
		3.85	0.96	900 ± 45		0.734 ± 0.037
		4.05	1.01	970 ± 50		0.720 ± 0.037
		4.25	1.06	1040 ± 70		0.713 ± 0.048
		4.38	1.09	950 ± 70		0.625 ± 0.046
		4.55	1.14	975 ± 75		0.608 ± 0.047
		4.88	1.22	1025 ± 100		0.589 ± 0.057
$^{58}\text{Ni} + ^{27}\text{Al}$	[69]	7.50	1.88	720 ± 50		0.302 ± 0.021
		28.00	6.07	300 ± 100		0.107 ± 0.036
$^{24}\text{Mg} + ^{63}\text{Cu}$	[70]	6.71	1.34	1050 ± 95		0.466 ± 0.042
		9.38	1.87	1130 ± 120		0.435 ± 0.046
		11.71	2.34	1015 ± 100		0.370 ± 0.037
		14.21	2.84	800 ± 130		0.284 ± 0.046
$^{48}\text{Ti} + ^{45}\text{Sc}$	[71]	15.98	3.99	650 ± 100		0.205 ± 0.031
$^{36}\text{Ar} + ^{58}\text{Ni}$	[15]	31.58	7.46	146 ± 35		0.048 ± 0.011
		40.03	9.46	65 ± 20		0.022 ± 0.007
		51.78	12.24	32 ± 25		0.011 ± 0.009
$^{16}\text{O} + ^{92}\text{Mo}$	[72]	11.70	1.48	1110 ± 101		0.427 ± 0.039

TABLE I. (*Continued.*)

System	Ref.	E_{in} (MeV/nucleon)	$E_{\text{c.m.}}/A_{\text{tot}}$ (MeV/nucleon)	σ_{fus} (mb)	CF (mb)	$\sigma_{\text{fus}}/\sigma_{\text{reac}}^T$
$^{32}\text{S} + ^{76}\text{Ge}$	[73]	4.94	1.03	1161 ± 101		0.620 ± 0.054
		5.56	1.16	1376 ± 101		0.644 ± 0.047
		6.19	1.29	1517 ± 96		0.646 ± 0.041
		6.81	1.42	1580 ± 96		0.628 ± 0.038
		7.03	1.47	1565 ± 98		0.610 ± 0.038
$^{40}\text{Ar} + ^{68}\text{Zn}$	[74]	14.60	3.40	990 ± 70		0.292 ± 0.021
		19.60	4.57	500 ± 60		0.145 ± 0.017
		27.55	6.42	200 ± 60		0.058 ± 0.018
		35.00	8.16	90 ± 40		0.027 ± 0.012
$^{52}\text{Cr} + ^{56}\text{Fe}$	[72]	5.10	1.27	943 ± 110		0.477 ± 0.056
$^{19}\text{F} + ^{93}\text{Nb}$	[75]	3.84	0.54	730 ± 62		0.731 ± 0.062
		5.00	0.70	1220 ± 93		0.728 ± 0.055
$^{64}\text{Zn} + ^{48}\text{Ti}$	[61]	35.00	8.57	100		0.029
		50.00	12.24	<20		0.006
$^{58}\text{Ni} + ^{58}\text{Ni}$	[15]	32.00	8.00	175 ± 20		0.050 ± 0.006
		40.50	10.13	85 ± 15		0.025 ± 0.004
		51.50	12.88	33 ± 20		0.010 ± 0.006
		63.50	15.88	14 ± 14		0.004 ± 0.004
$^{18}\text{O} + ^{100}\text{Mo}$	[76]	5.56	0.72	1588 ± 70		0.771 ± 0.034
		8.33	1.08	1644 ± 70		0.621 ± 0.026
		9.39	1.21	1563 ± 70		0.565 ± 0.025
		10.28	1.33	1700 ± 70		0.598 ± 0.025
		12.06	1.56	1775 ± 70		0.601 ± 0.024
$^{78}\text{Kr} + ^{40}\text{Ca}$	[77]	5.50	1.23	986 ± 110		0.525 ± 0.059
$^{82}\text{Kr} + ^{40}\text{Ca}$	[77]	5.50	1.21	824 ± 97		0.420 ± 0.049
$^{12}\text{C} + ^{124}\text{Sn}$	[78]	30.00	2.41	728 ± 75		0.255 ± 0.026
		49.00	3.94	344 ± 75		0.127 ± 0.028
		84.00	6.76	20 ± 10		0.008 ± 0.004
$^{14}\text{N} + ^{124}\text{Sn}$	[78]	10.00	0.91	1277 ± 75		0.498 ± 0.029
		20.00	1.82	1112 ± 75		0.373 ± 0.025
		30.00	2.73	860 ± 120		0.289 ± 0.040
$^{20}\text{Ne} + ^{124}\text{Sn}$	[78]	20.00	2.39	990 ± 100		0.295 ± 0.030
		30.00	3.59	651 ± 90		0.193 ± 0.027
$^{40}\text{Ar} + ^{109}\text{Ag}$	[80]	4.22	0.83	455 ± 70		0.418 ± 0.064
		4.93	0.97	920 ± 140		0.550 ± 0.084
		5.90	1.16	1170 ± 170		0.520 ± 0.076
		7.20	1.41	1270 ± 180		0.460 ± 0.065
		8.43	1.65	975 ± 160		0.316 ± 0.052
	[81]	7.20	1.41	1300		0.471
		8.40	1.65	1255 ± 125		0.408 ± 0.041
		27.40	5.38	480		0.121
$^{84}\text{Kr} + ^{65}\text{Cu}$	[80]	5.88	1.45	1390 ± 320		0.569 ± 0.131
		7.19	1.77	1560 ± 180		0.523 ± 0.060
$^{40}\text{Ar} + ^{116}\text{Sn}$	[84]	4.63	0.88	700 ± 70		0.532 ± 0.053
		4.63	0.88	700 ± 70		0.532 ± 0.053
		5.50	1.05	829 ± 83		0.426 ± 0.043
		6.78	1.29	838 ± 102		0.327 ± 0.040
		8.48	1.62	1123 ± 100		0.365 ± 0.033
$^{40}\text{Ar} + ^{121}\text{Sb}$	[85]	4.97	0.93	1045 ± 110		0.648 ± 0.068
		5.65	1.05	1040 ± 70		0.505 ± 0.034
		7.50	1.40	1130 ± 80		0.396 ± 0.028
	[80]	7.05	1.32	1130 ± 200		0.418 ± 0.074

TABLE I. (*Continued.*)

System	Ref.	E_{in} (MeV/nucleon)	$E_{\text{c.m.}}/A_{\text{tot}}$ (MeV/nucleon)	σ_{fus} (mb)	CF (mb)	$\sigma_{\text{fus}}/\sigma_{\text{reac}}^T$
$^{16}\text{O} + ^{146}\text{Nd}$	[86]	10.06	0.90	1644 ± 122		0.625 ± 0.046
$^{132}\text{Xe} + ^{30}\text{Si}$	[87]	5.40	0.81	995 ± 30		0.579 ± 0.017
		5.90	0.89	1096 ± 60		0.548 ± 0.030
		6.60	1.00	1169 ± 90		0.504 ± 0.039
		7.50	1.13	1274 ± 130		0.484 ± 0.049
		8.20	1.24	1285 ± 140		0.455 ± 0.050
$^{40}\text{Ar} + ^{124}\text{Sn}$	[78]	24.00	4.43	812 ± 90		0.196 ± 0.022
		27.00	4.98	528 ± 75		0.128 ± 0.018
$^{14}\text{N} + ^{154}\text{Sm}$	[88]	35.00	2.67	1476		0.461
	[89]	35.00	2.67	1270 ± 180		0.397 ± 0.056
		100.00	7.64	630 ± 70		0.220 ± 0.024
		130.00	9.93	540 ± 90		0.193 ± 0.032
		155.00	11.84	460 ± 120		0.166 ± 0.043
$^{14}\text{N} + ^{159}\text{Tb}$	[90]	22.07	1.64	1571 ± 204		0.495 ± 0.064
	[89]	35.00	2.60	1200 ± 160		0.377 ± 0.050
		100.00	7.44	720 ± 100		0.253 ± 0.035
$^{16}\text{O} + ^{159}\text{Tb}$	[91]	14.00	1.16	1932 ± 200		0.638 ± 0.066
	[88]	25.00	2.08	1720		0.516
$^{20}\text{Ne} + ^{159}\text{Tb}$	[92]	8.00	0.79	1352 ± 72		0.584 ± 0.031
		10.00	0.99	1581 ± 86		0.569 ± 0.031
		13.00	1.29	1600 ± 80		0.505 ± 0.025
		16.00	1.59	1683 ± 91		0.498 ± 0.027
$^{58}\text{Ni} + ^{124}\text{Sn}$	[93]	3.96	0.86	19 ± 3		<0
		4.12	0.89	95 ± 11		0.405 ± 0.047
		4.28	0.93	190 ± 27		0.417 ± 0.059
		4.66	1.01	405 ± 52		0.441 ± 0.057
		5.00	1.09	465 ± 62		0.365 ± 0.049
$^{20}\text{Ne} + ^{165}\text{Ho}$	[94]	30.00	2.89	2355 ± 140		0.638 ± 0.038
$^{20}\text{Ne} + ^{169}\text{Tm}$	[92]	8.00	0.76	1421 ± 100		0.614 ± 0.043
		10.00	0.95	1589 ± 85		0.566 ± 0.030
		13.00	1.23	1624 ± 74		0.503 ± 0.023
		16.00	1.51	1638 ± 74		0.474 ± 0.021
$^{12}\text{C} + ^{182}\text{W}$	[95]	10.08	0.58	1065 ± 105		0.446 ± 0.044
		13.92	0.81	1614 ± 160		0.568 ± 0.056
$^{19}\text{F} + ^{175}\text{Lu}$	[95]	7.11	0.63	1131 ± 110		0.544 ± 0.053
		9.68	0.86	1378 ± 140		0.492 ± 0.050
$^{40}\text{Ar} + ^{154}\text{Sm}$	[84]	5.53	0.90	840 ± 75		0.471 ± 0.042
		6.80	1.11	998 ± 95		0.393 ± 0.037
		8.50	1.39	1563 ± 310		0.493 ± 0.098
$^{14}\text{N} + ^{181}\text{Ta}$	[88]	35.00	2.33	1453		0.433
$^{16}\text{O} + ^{181}\text{Ta}$	[91]	14.00	1.04	1974 ± 200		0.638 ± 0.065
	[88]	25.00	1.87	1700		0.488
$^{40}\text{Ar} + ^{164}\text{Dy}$	[84]	5.53	0.87	875 ± 80		0.523 ± 0.048
		6.80	1.07	968 ± 77		0.394 ± 0.031
		8.48	1.34	1225 ± 215		0.392 ± 0.069
$^{24}\text{Mg} + ^{181}\text{Ta}$	[96]	11.25	1.16	1360 ± 160		0.439 ± 0.052
		13.96	1.44	1090 ± 130		0.316 ± 0.038
		14.17	1.46	1140 ± 130		0.329 ± 0.037
$^{40}\text{Ar} + ^{165}\text{Ho}$	[85]	5.65	0.89	800 ± 90		0.476 ± 0.054
		7.50	1.18	1350 ± 140		0.495 ± 0.051
	[96]	7.00	1.10	1320 ± 200		0.527 ± 0.080
		7.88	1.24	1095 ± 130		0.381 ± 0.045

TABLE I. (*Continued.*)

System	Ref.	E_{in} (MeV/nucleon)	$E_{\text{c.m.}}/A_{\text{tot}}$ (MeV/nucleon)	σ_{fus} (mb)	CF (mb)	$\sigma_{\text{fus}}/\sigma_{\text{reac}}^T$
$^{12}\text{C} + ^{197}\text{Au}$	[97]	8.50	1.33	1260 ± 190		0.407 ± 0.061
		9.77	1.54	1450 ± 180		0.422 ± 0.052
$^{14}\text{N} + ^{197}\text{Au}$	[89]	86.00	4.65	340 ± 40		0.111 ± 0.013
		35.00	2.17	1720 ± 200		0.502 ± 0.058
$^{14}\text{N} + ^{197}\text{Au}$		100.00	6.19	950 ± 100		0.303 ± 0.032
		130.00	8.05	650 ± 80		0.211 ± 0.026
		155.00	9.60	590 ± 120		0.193 ± 0.039
		14.00	0.97	2030 ± 160		0.657 ± 0.052
$^{16}\text{O} + ^{197}\text{Au}$	[91]	107.00	7.43	360 ± 40		0.110 ± 0.012
		7.50	0.63	1370 ± 125		0.715 ± 0.065
$^{20}\text{Ne} + ^{197}\text{Au}$	[98]	11.00	0.92	1900 ± 300		0.653 ± 0.103
		14.50	1.21	2265 ± 200		0.667 ± 0.059
		20.00	1.67	2165 ± 400		0.586 ± 0.108
		30.00	2.51	1600 ± 320		0.414 ± 0.083
$^{20}\text{Ne} + ^{209}\text{Bi}$	[99]	30.00	2.39	2200 ± 450		0.560 ± 0.115
$^{40}\text{Ar} + ^{197}\text{Au}$	[84]	5.47	0.77	518 ± 46		0.481 ± 0.043
		6.75	0.95	794 ± 142		0.383 ± 0.068
		8.48	1.19	1577 ± 208		0.539 ± 0.071
		5.68	0.80	550 ± 85		0.435 ± 0.067
		6.20	0.87	810 ± 125		0.478 ± 0.074
		8.40	1.18	1451 ± 150		0.501 ± 0.052
		8.57	1.20	1350 ± 220		0.456 ± 0.074
		30.00	1.66	1800		0.498
$^{40}\text{Ar} + ^{238}\text{U}$	[85]	6.25	0.77	516 ± 150		0.362 ± 0.105
		7.50	0.92	1030 ± 120		0.444 ± 0.052
		7.50	0.92	1220		0.526 ± 0.000
		10.40	1.28	1400		0.397 ± 0.000
	[103]	8.50	1.05	1020 ± 150		0.360 ± 0.053

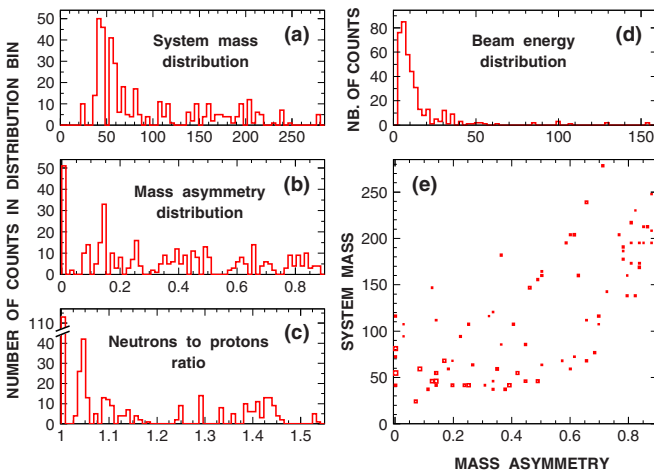


FIG. 2. (Color online) Statistics of 382 fusion cross-section data points (CF and CF + IF) as a function of (a) system mass A_{tot} , (b) mass asymmetry μ , (c) system neutron-to-proton ratio $N_{\text{tot}}/Z_{\text{tot}}$, and (d) reaction incident energy E_{in} , while (e) shows the correlation between A_{tot} and μ . The size of squares in the scatter plot (e) is proportional to the number of data points within the crossed bins.

of low μ data for systems of $A_{\text{tot}} \gtrsim 120$ a.m.u. Interestingly enough, a projection onto the μ axis [see Fig. 2(b)] shows that the data points are relatively uniformly distributed over the asymmetry μ domain except for the symmetric $\mu = 0$ systems, which are more abundantly populated. For the other observables most of σ_{fus} data lie in a relatively narrow zone of the observable domain. The σ_{fus} values corresponding to isospin symmetric systems ($N_{\text{tot}}/Z_{\text{tot}} = 1$) represent almost one third of the ensemble of data points. The mass distribution is dominated by lighter systems with $A_{\text{tot}} \approx 50 \pm 15$. This band of A_{tot} covers a large span of μ [see Fig. 2(e)], although the coverage in E_{in} is quite restricted to lower energies. As already mentioned, Fig. 2(d) clearly displays to which extent are fusion data scarce for all E_{in} above $\sim 20A$ MeV. Finally, let us comment that the atomic numbers of the reacting nuclei are such that any data point is much below the compound-nucleus formation limit which has been estimated (see Eq. (16) in Ref. [1]) and experimentally confirmed [23] to occur when the product $Z_p \times Z_t$ of the projectile and target atomic charges exceeds $\sim 2500-2700$.

At a first glance the fusion data of Fig. 1 seems to be spread out over the σ_{fus} vs E_{in} plane. A more detailed

examination of the data points suggests that most of them are lying within two relatively narrow crossing strips: a narrow arclike zone dominated by lighter systems (blue-cyan-green symbols) and an almost vertical band of heavier systems (red-orange-dark-red symbols). The fact that systems of low and high A_{tot} do not fall together is expected due to the known dependence of the fusion cross section on the system size. We are interested in a presentation of the above raw σ_{fus} results which would allow us to pin down a possible functional dependence able to commonly describe a large majority of the data of Table I in the spirit of Fig. 8 of Ref. [15]. Establishing such an universal law would be of great help in, for instance, checking and mapping model predictions of fusion processes and, consequently, in elucidating the role of dynamical and thermodynamical contributions in nuclear reactions at these energies.

III. DATA RENORMALIZATION

One accounts for the proportionality of cross section to the size of a reaction system by renormalizing σ_{fus} by (total) reaction cross section σ_{reac} at the same E_{in} . Accurate measurement of the total σ_{reac} is rather hard so these data are scarce and, moreover, often published without reporting the uncertainty on (see Table II). Therefore, one commonly resorts to phenomenological approaches to calculate σ_{reac} , a solution which suffers for its own uncertainties and ambiguities.

A. Total reaction cross section

Several parametrizations are used to calculate σ_{reac} in the energy range of our concern [3,24,104–108]. A comparison between some of the most used empirical formulas is displayed in Fig. 3. Shown are the ratios of the values calculated with the formulas of Refs. [3,104,105] to the most recent one due to Tripathi [24] for the systems and energies of Table I and Fig. 1 as a function of the so-called system available energy defined as the center-of-mass energy per nucleon

$$E_{\text{avail}} = \frac{E_{\text{c.m.}}}{A_{\text{tot}}} = \frac{E_{\text{lab}}}{A_p} \frac{A_p A_t}{(A_p + A_t)^2}. \quad (1)$$

Historically the first, the Bass-formula [3] [see upper part of Fig. 3(a)] systematically predicts larger σ_{reac} than the one due to Tripathi, a behavior strongly enhanced by the increase of energy. In the lower part of Fig. 3(a) is shown the ratio of the Kox [104] to Tripathi [24] σ_{reac} . To extend the applicability of the Kox formula down to a few A_p MeV we have modified it similar to the way as Shen *et al.* [105] did. Compared to the above Bass-Tripathi case, the ratio of the Kox-Tripathi results displays a much weaker dependence on the system characteristics: The difference regarding μ or $N_{\text{tot}}/Z_{\text{tot}}$ is strongly reduced and at most amounts to about 15% as a function of A_{tot} . For $E_{\text{c.m.}}/A_{\text{tot}} > 2$ the ratio is below ≈15%, whereas it diverges for decreasing energy, especially below $E_{\text{c.m.}}/A_{\text{tot}} \approx 1$ MeV/nucleon. In other words, these two approaches [24,104] essentially differ on the definition of nuclear radii they use and thus on the position of the deduced barrier for fusion. Figure 3(b) shows the ratio of σ_{reac} according to Shen [105] and Tripathi [24]. These two

TABLE II. Experimentally deduced reaction cross sections σ_{reac} either by summing up the contribution of measured individual reaction channels (in the third column labeled “Summed”) or from a measured elastic scattering and the use of optical model (labeled “OM”), whereas in one case the ratio $\sigma_{\text{fus}}/\sigma_{\text{reac}}$ has been stated in the original work (labeled “Ratio”). All data given include the reference to original work, the method used in obtaining σ_{reac} , the incident energy per nucleon E_{in} , and the σ_{reac} .

System	Ref.	Method	E_{in} (MeV/nucleon)	σ_{reac} (mb)
$^{14}\text{N} + ^{12}\text{C}$	[25]	Summed	4.29	1252
		Summed	6.16	1314
		Summed	7.59	1390
		Summed	10.39	1441
		Summed	11.94	1311
		Summed	12.72	1408
	[26]	OM	11.29	1460
		OM	17.70	1450
	[27]	Summed	3.40	1186 ± 120
		Summed	5.74	1523 ± 150
		Summed	6.10	1549 ± 150
		Summed	6.85	1739 ± 160
		Summed	7.80	1613 ± 140
$^{20}\text{Ne} + ^{16}\text{O}$	[27]	Summed	3.40	1159 ± 103
		Summed	5.85	1665 ± 145
		Summed	6.30	1623 ± 140
		Summed	7.00	1705 ± 155
		Summed	7.80	1722 ± 90
$^{32}\text{S} + ^{12}\text{C}$	[39]	Summed	3.40	1120 ± 70
		Summed	4.10	1300 ± 80
	[39]	Summed	4.53	1446 ± 60
	[40]	Summed	5.00	1309 ± 80
	[43]	OM	6.00	1646
		OM	7.50	1805
		OM	9.00	1794
		OM	14.50	1921
$^{35}\text{Cl} + ^{12}\text{C}$	[44]	OM	3.57	1115
	[44]	OM	4.40	1417
	[45]	OM	5.71	1619
$^{16}\text{O} + ^{40}\text{Ca}$	[47]	Summed	8.73	1981
		Summed	13.38	2123
	[48]	OM	13.38	2268
	[48]	Summed	13.38	2110
$^{40}\text{Ar} + ^{40}\text{Ca}$	[64]	OM	4.02	1462
		OM	4.75	1736
		OM	5.90	2038
		OM	6.83	2202
$^{16}\text{O} + ^{92}\text{Mo}$	[72]	Summed	11.70	2320 ± 110
$^{32}\text{S} + ^{76}\text{Ge}$	[73]	OM	4.94	1970
		OM	5.56	2120
		OM	6.19	2210
		OM	6.81	2320
		OM	7.03	2340
$^{40}\text{Ar} + ^{68}\text{Zn}$	[74]	OM	14.60	3113
		OM	19.60	4065
		OM	27.55	3146
		OM	35.00	2395

TABLE II. (*Continued.*)

System	Ref.	Method	E_{in} (MeV/nucleon)	σ_{reac} (mb)
$^{52}\text{Cr} + ^{56}\text{Fe}$	[72]	Summed	5.10	1260 ± 80
$^{19}\text{F} + ^{93}\text{Nb}$	[75]	Summed	5.00	1510 ± 90
$^{12}\text{C} + ^{124}\text{Sn}$	[78]	OM	30.00	3563
		OM	49.00	3386
$^{14}\text{N} + ^{124}\text{Sn}$	[78]	OM	10.00	2527
		OM	20.00	3231
		OM	30.00	3466
$^{20}\text{Ne} + ^{124}\text{Sn}$	[78]	OM	20.00	3669
		OM	30.00	3416
$^{40}\text{Ar} + ^{109}\text{Ag}$	[80]	Summed	4.22	859 ± 120
		Summed	4.93	1410 ± 140
		Summed	5.90	1830 ± 180
		Summed	7.20	2110 ± 220
		Summed	8.43	2270 ± 190
	[82]	Summed	8.40	2700
$^{84}\text{Kr} + ^{65}\text{Cu}$	[80]	OM	7.19	2430
$^{40}\text{Ar} + ^{116}\text{Sn}$	[84]	OM	8.48	2483
$^{40}\text{Ar} + ^{121}\text{Sb}$	[80]	OM	7.05	2210
$^{132}\text{Xe} + ^{30}\text{Si}$	[87]	Summed	5.40	1403 ± 140
		Summed	5.90	1656 ± 165
		Summed	6.60	1938 ± 190
		Summed	7.50	2222 ± 220
		Summed	8.20	2397 ± 240
$^{40}\text{Ar} + ^{124}\text{Sn}$	[78]	OM	24.00	4060
		OM	27.00	4130
$^{58}\text{Ni} + ^{124}\text{Sn}$	[93]	Summed	3.96	150 ± 15
		Summed	4.12	310 ± 25
		Summed	4.28	615 ± 45
		Summed	4.66	1025 ± 75
		Summed	5.00	1345 ± 95
$^{20}\text{Ne} + ^{165}\text{Ho}$	[94]	Ratio	30.00	3360 ± 270
$^{40}\text{Ar} + ^{154}\text{Sm}$	[82]	OM	8.40	2565
	[84]	OM	8.50	2565
$^{40}\text{Ar} + ^{164}\text{Dy}$	[84]	OM	8.48	2530
$^{20}\text{Ne} + ^{197}\text{Au}$	[99]	OM	30.00	3150
$^{20}\text{Ne} + ^{209}\text{Bi}$	[99]	OM	30.00	3250
$^{40}\text{Ar} + ^{197}\text{Au}$	[82]	OM	8.40	2400
	[101]	OM	8.57	2407

parametrizations of σ_{reac} give, within a few percent, the same result: The dependence on the system characteristics is almost the same and that on energy is remarkably similar as one can infer from the histograms of Fig. 3(c), which represent the projection of Fig. 3(b) onto its ordinate. The mean value of the distribution is 0.999 ± 0.041 over the all 346 data points of the column 5 of Table I and 1.014 ± 0.035 over 256 points with $E_{\text{c.m.}}/A_{\text{tot}} > 1.06$, an energy cut which is clarified and justified later on.

The global features of the ratios of experimental and model σ_{reac} for the four used formulas are shown in Fig. 4 and

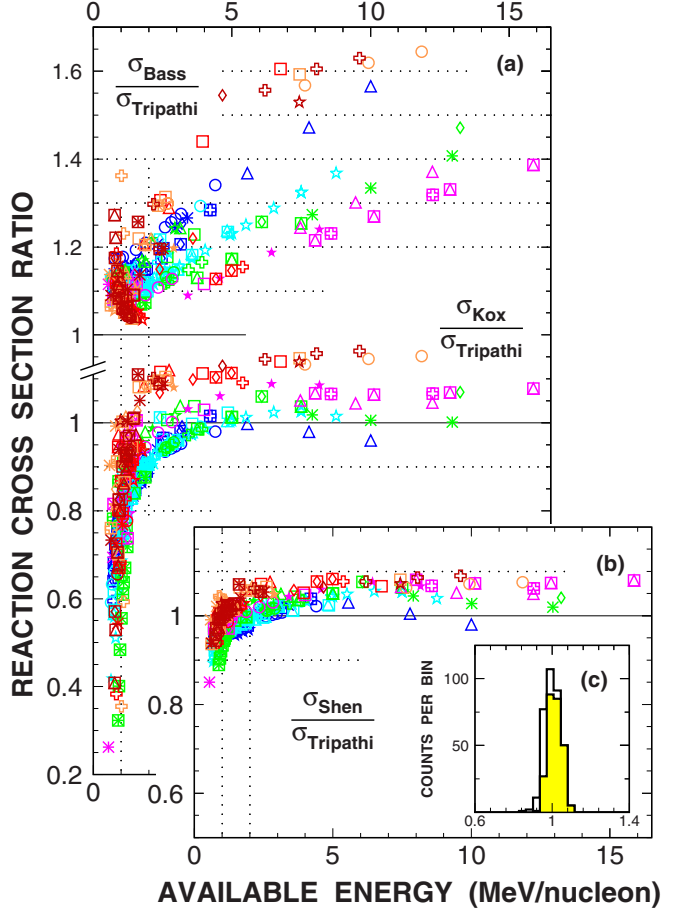


FIG. 3. (Color online) Ratios of reaction cross sections calculated with the Bass [3], Kox [104] (a), and Shen [105] (b) formulas vs that of Tripathi [24] at energies of fusion data of Table I. Inset (c) shows the projection of the Shen-Tripathi ratio onto the ordinate axis taking either all points (hollow histogram) or those of energy $E_{\text{c.m.}}/A_{\text{tot}} > 1.06$ MeV/nucleon (filled histogram). Meaning of the symbols and levels of gray (colors online) are listed in Fig. 1.

Table III. Besides the 85 experimental $\sigma_{\text{reac}}^{\text{exper}}$ values listed in Table II we also used the 49 points of Tables I and II of Ref. [104]. From the median and standard deviation values of the ratio $\sigma_{\text{reac}}^{\text{exper}}/\sigma_{\text{reac}}^{\text{theory}}$ over the all used experimental data, it becomes obvious that the Tripathi [24] and Shen [105] formulas compare more favorably with the experimental data

TABLE III. Statistics of the ratios of experimental to the four studied empirical model reaction cross section for the 134 data values of 46 reaction systems listed in both Table II and Ref. [104]. Values in parentheses are for 116 points satisfying the condition $E_{\text{c.m.}}/A_{\text{tot}} > 1.06$ MeV/nucleon.

Reaction model	Median	Standard deviation
Bass [3]	0.72 (0.72)	0.15 (0.15)
Kox [104]	1.02 (1.00)	0.26 (0.24)
Shen [105]	0.94 (0.94)	0.11 (0.10)
Tripathi [24]	0.95 (0.95)	0.12 (0.12)

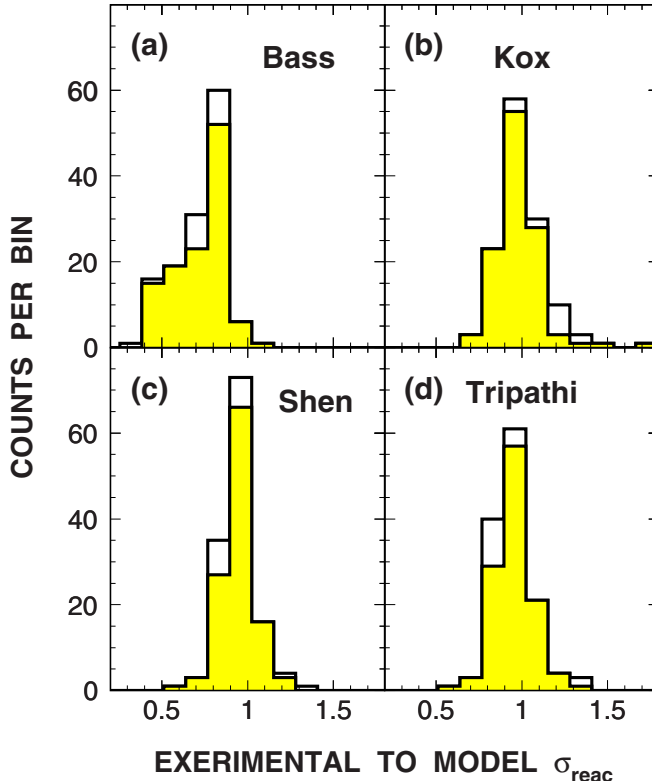


FIG. 4. (Color online) Histograms of the ratios of experimental and model reaction cross sections using (a) Bass [3], (b) Kox [104], (c) Shen [105], and (d) Tripathi [24] formulas, respectively. Hollow histograms refer to all the used experimental reaction data and those filled to the data fulfilling the condition $E_{\text{c.m.}}/A_{\text{tot}} > 1.06 \text{ MeV/nucleon}$.

than the Kox one [104], although the Kox formula has been explicitly adjusted to fit a large portion of the ensemble of the data used in our comparison. Corroborating the observation of Fig. 3(a) the Bass parametrization of σ_{reac} overestimates, on average, the experimental σ_{reac} by about 30%.

From the above discussion follows that one may use either Tripathi or Shen formula without clear preference. All the analysis presented in the rest of this paper has been carried out with the both parameterizations of σ_{reac} . The obtained results are the same within a few per mill. In the rest of this work we have adopted to present results with the Tripathi formula σ_{reac}^T for reaction cross section [24]. Note that σ_{reac}^T depends on the root-mean-square charge radii of nuclei for which we used the tabulated values of Ref. [109]. The analysis of the subset of 48 reaction systems with a total of 238 fusion-evaporation cross sections and which has been published in the recent paper [21] has been carried out with the Shen formula [105]. An interested reader may consult it to become aware to which extent these two normalizations give much the same results.

B. Scaling of cross section

Figure 5 displays $\sigma_{\text{fus}}^N = \sigma_{\text{fus}}/\sigma_{\text{reac}}^T$, i.e., the experimental fusion cross section of Fig. 1 normalized by the reaction cross section derived from the empirical Tripathi formula [24]. The σ_{fus}^N values are also listed in the last column of Table I.

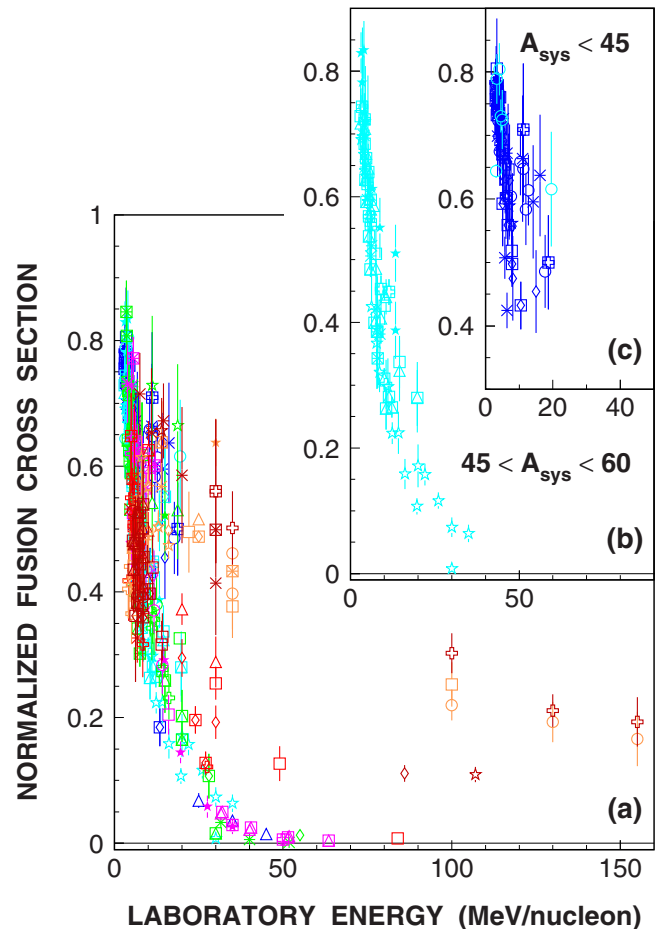


FIG. 5. (Color online) Normalized fusion cross sections σ_{fus}^N plotted as a function of the laboratory energy per nucleon E_{in} . To better resolve the stacked points, panels (c) and (b) repeat the data subsets for $A_{\text{tot}} \leq 44$ and $46 \leq A_{\text{tot}} \leq 59$, respectively. The meaning of the symbols and levels of gray (colors online) may be inferred from Fig. 1.

As expected, the renormalization of σ_{fus} results in a strongly reduced number of spread-out fusion data points. The arclike feature of the majority of the fusion data is clearly visible involving all color codes, i.e., the full range of A_{tot} . Note a massive pileup of points for $E_{\text{in}} < 10A$ MeV that is made visible by zooming on low- A_{tot} data subsets, shown in Figs. 5(b) and 5(c). One should bear in mind, however, that this presentation compresses the width of the arc and a zoom on $E_{\text{in}} = 0\text{--}50A$ MeV would reveal a real width of that arclike zone.

C. Scaling of energy

Figure 6 shows the normalized σ_{fus}^N for the eight mass symmetric or nearly mass symmetric systems and the corresponding 49 points from Table I. A very regular correlation of σ_{fus}^N with energy is obvious. One may raise the question of whether the still-present discrepancy in the energy dependence between mass-symmetric and mass-nonsymmetric systems may be reduced. Indeed, by specifying abscissas in units of the so-called system available energy of Eq. (1), i.e.,

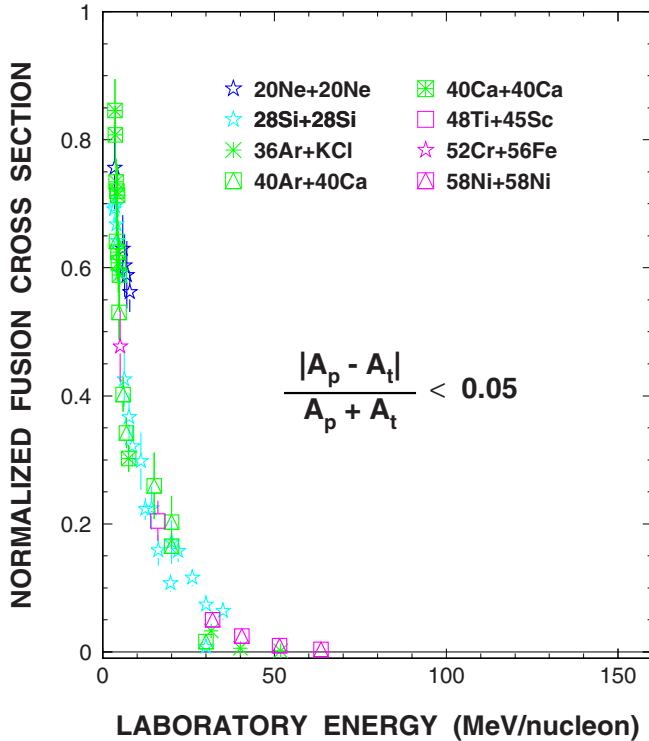


FIG. 6. (Color online) Same as Fig. 5 but for mass symmetric systems.

$E_{\text{c.m.}}/A_{\text{tot}}$, one does express the mass asymmetric systems on the same footing with those which are mass symmetric. Such a coordinate scaling greatly eases the comparison of various systems with each other. The obtained result is displayed in Fig. 7. At a mere glance, many data points which have been strongly scattered in the two previous presentations of the fusion data (cf. in Figs. 1 and 5) are now lying in a much narrower zone of the σ_{fus}^N vs $E_{\text{c.m.}}/A_{\text{tot}}$ plane. Note that relative to the two previous figures the abscissa is expanded by a factor of 10, displaying the detailed structure of the arclike zone. For $E_{\text{c.m.}}/A_{\text{tot}} \lesssim 2$ the arclike feature of this zone is less straightforward, but one has to keep in mind that at low energies the experimental error bars are generally larger than the average errors and their relative values are higher than 15% (see also the inset in Fig. 8). A large portion of these points is coming from fusion-fission contribution which has some additional inherent uncertainty, which is discussed later. Also, one should not disregard the fact discussed in Sec. III A that reaction models mostly differ at low energies due to the problem of the correct attribution of interaction radius to a colliding system. Although the Tripathi formula includes terms accounting for the mass asymmetry and isospin of the system, the pertinence of the σ_{reac} description for a large number of systems and energies may substantially vary from one system to another. The irregularities in the quality of the description of data were clearly observed by applying the four mentioned model σ_{reac} in order to examine their impact on the normalization of fusion yields.

Several systems or groups of data, however, do not follow the possible common rule we are seeking to establish. Indeed,

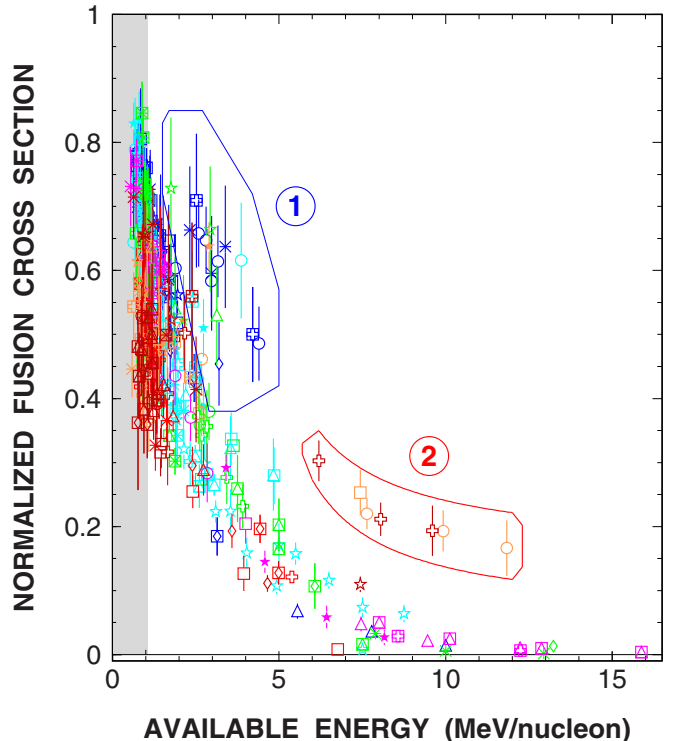


FIG. 7. (Color online) Normalized fusion cross sections σ_{fus}^N plotted as a function of the center-of-mass energy per nucleon $E_{\text{c.m.}}/A_{\text{tot}}$. The meaning of the symbols and levels of gray (colors online) may be inferred from Fig. 1. A light-gray band for $E_{\text{c.m.}}/A_{\text{tot}} < 1.06$ MeV/nucleon delimits a portion of the data set which is of no particular relevance in the present study because we focus on fusion region III and fusion disappearance. For the discussion on the groups of data labeled by ① and ②, see text.

besides the arclike zone discussed above and in Figs. 1 and 5, which now becomes much less dominated by lighter systems (blue-cyan-green symbols), one may identify two separate groups of data, labeled ① and ② in Fig. 7. Group ① contains 22 rather scattered fusion data points with large error bars. In contrast, group ② displays a nicely regular bandlike shape lying above and roughly parallel to the main arclike zone. It contains 7 data points, all of them belonging to the same measurement of 10 fusion data [89]. These points are lying apart from all others and tend to a constant value of σ_{fus}^N when energy increases. They come from the ^{14}N -induced reactions on ^{154}Sm (open circles), ^{159}Tb (open squares), and ^{197}Au (open plus signs) at $35A$, $100A$, $130A$, and $155A$ MeV. The reported σ_{fus} for $E_{\text{in}} \geq 100A$ MeV are several times larger than other data at similar $E_{\text{c.m.}}/A_{\text{tot}}$. In particular, these results differ from those of Ref. [78], reporting on the fusion results of the ^{12}C , ^{14}N , ^{20}Ne , and ^{40}Ar projectiles of energies up to $49A$ MeV that impinge on the ^{124}Sn target, i.e., systems with comparable A_{tot} and μ and with partially overlapping $E_{\text{c.m.}}/A_{\text{tot}}$. The data of these two measurements at $E_{\text{in}} = 35A$ and $30A$ MeV, respectively, do not differ by more than about a factor two (cf. in Table I) but their trends with the increase of energy are substantially different. In the latter case the evaporation fusion component has been measured only, whereas by systematics a

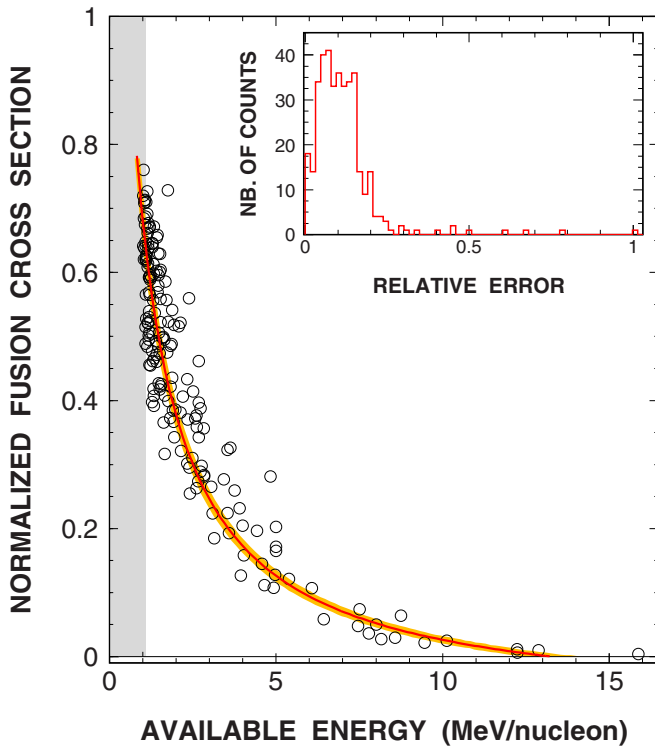


FIG. 8. (Color online) σ_{fus}^N plotted as a function of $E_{\text{c.m.}}/A_{\text{tot}}$ for those data points which survived the iterative fitting procedure. The curve is due to a fit with the homographic function (4) restricted to 256 data points and 78 reaction systems lying outside the light-gray band. (For the explanation of the light-gray band see the caption of Fig. 7 and text.) The background band around the best fit curve is due to the errors on the fit parameters provided by the used code [111]. The histogram in the inset shows the distribution of relative errors of experimental fusion cross sections $\Delta\sigma_{\text{fus}}^N$ when $\Delta\sigma_{\text{fus}}$ are normalized by the Tripathi reaction cross section σ_{reac}^T .

more or less significant fission component has been expected too. Anyhow, adding the expected fission contribution to fusion to these σ_{fus} data with the ^{124}Sn target would probably move these data from the border to the middle of the main arclike zone of fusion data of the σ_{fus}^N vs $E_{\text{c.m.}}/A_{\text{tot}}$ plane without bringing them significantly closer to the ^{14}N -induced data of Ref. [89].

The data of group ② suggests persistence of fusion beyond the measured energies. In a recent work [110] we have shown that the $\text{N} + \text{Sm}$ reaction is driven by fundamentally different mechanisms at 35A MeV and above 100A MeV. At 35A MeV the reaction mechanism is compatible with fusion, whereas above 100A MeV the reaction geometry and a mechanism reminiscent of the participant-spectator [112] picture governs the reaction process. In addition, a simple estimation of cross section relying solely on the geometry of the reaction entrance channel correctly reproduces the experimental values of the group ② yields extrapolated asymptotically [110].

In group ①, the fusion data which are far off a global behavior are the highest energy points of the measurements $^{14}\text{N} + ^{12}\text{C}$ [25,26] (6 points), $^{28}\text{Si} + ^{12}\text{C}$ [31] (3 points), the last point of the $^{12}\text{C} + ^{27}\text{Al}$, ^{48}Ti [29], and $^{16}\text{O} + ^{40}\text{Ca}$ [47],

and all points of measurements $^{14}\text{N} + ^{27}\text{Al}$, ^{52}Cr , ^{58}Ni [33] (6 points), as well as the single-data-point measurements $^{32}\text{S} + ^{12}\text{C}$ [41], $^{14}\text{N} + ^{154}\text{Sm}$ [88], $^{20}\text{Ne} + ^{165}\text{Ho}$ [94], and $^{20}\text{Ne} + ^{209}\text{Bi}$ [99] (see Table I for details). The lower energy $^{14}\text{N} + ^{58}\text{Ni}$ point [33] and the last one ($^{20}\text{Ne} + ^{209}\text{Bi}$ [99]) have a so large error that the 3σ uncertainty includes these points into the main systematics (cf. in Fig. 8). These 22 points represent less than 6% of the ensemble of the σ_{fus} data presented in this work. A careful examination of the original works does not allow us to identify a possible deficiency or inadequacy in the design or in the accomplishment of these experiments. However, a scrutiny of Table I evidences in some cases large discrepancies in the reported results. The extreme example is at $E_{\text{in}} = 30\text{A}$ MeV of the Si + Si system where two measurements [51,53] differ by a factor of 9.2. For this, the most abundantly measured among the studied fusion systems (5 measurements with 22 σ_{fus} data [49–53]), a large discrepancy of a factor 1.6 also exists between yields at $E_{\text{in}} = 19.7\text{A}$ [51] and 20A MeV [53]. These examples show that similar errors in the absolute cross sections may be present in the above discussed cases. Let us also remember that at these relatively high energies fusion is in competition with deep inelastic processes. At the time of these experiments the knowledge on the deep inelastic process has been far less complete. One knows today that it is rather hard to disentangle the contribution of fusionlike mechanisms from that of damped nonthermalized processes involving large momentum transfer of noncoincident measurements, such as those applied at that time. This may be at the origin of the observed departure of at least some of the above results from the general feature of the fusion data. Finally, we note that in their study of the fusion excitation function for 54 individual fusion reactions in the σ_{fus} vs $1/E_{\text{c.m.}}$ representation Giordano *et al.* [9] have achieved very satisfactory fit to all reactions over the whole available data set except for the portion of the $^{14}\text{N} + ^{12}\text{C}$ [25,26] data with $E_{\text{c.m.}}/A_{\text{tot}} > 1.8$ MeV/nucleon (cf. in Fig. 1 of Ref. [9]), i.e., for the same points of the reaction we are discussing about.

IV. UNIVERSAL FUSION EXCITATION FUNCTION

A. Global fusion data

In the previous section we have discussed the departure of a few renormalized and energy scaled fusion data of Fig. 7 from the global behavior of the data. Assuming that this discussion relies on solid grounds it is justified to attempt fitting the ensemble of the σ_{fus}^N data (values reported in the last column in Table I) by allowing the fit procedure to iteratively exclude those data points which are outside the best fit result by more than three times the corresponding experimental error bar.¹

According to the strong absorption model both σ_{fus} and σ_{reac} may be approximated by the same functional form

$$\sigma(E) = \pi R^2 \left(1 - \frac{V}{E}\right), \quad (2)$$

¹In case of unreported experimental error it has been assumed to be 20% of the corresponding cross-section value.

TABLE IV. Values of the best fit coefficients a , b , and c of the homographic function (4) for the full fusion-data set, the evaporation-residue subset, and the subset of complete fusion data, with and without energy cut, respectively.

Data set without energy cut	a	b	c
All incomplete fusion data	-0.0964	1.3473	0.8178
Fusion-evaporation data	-0.0997	1.3925	0.8180
Complete fusion data	-0.2289	1.5456	0.5787
Fusion region III data			
All incomplete fusion data	-0.0842	1.1602	0.5162
Fusion-evaporation data	-0.0799	1.0993	0.3944
Complete fusion data	-0.2118	1.5385	0.7023

in which the cross section depends on the inverse of the energy E while the radius R and the potential depth V may be considered constants for a given system (see, e.g., Refs. [1,24,113]). Thus, for the normalized cross section one may write

$$\sigma_{\text{fus}}^N(E_{\text{c.m.}}) = \frac{a_1 + \frac{b_1}{E_{\text{c.m.}}}}{a_2 + \frac{b_2}{E_{\text{c.m.}}}}, \quad (3)$$

where a_i and b_i ($i = 1, 2$) are constants. Equation (3) is equivalent to a homographic function in energy $f(x)$ which we take to be our probe function

$$f(x) = a + \frac{b}{c + x}, \quad (4)$$

with $x = E_{\text{c.m.}}/A_{\text{tot}}$ and where a , b , and c are fit parameters. The fit was carried out with the MINUIT package of the CERN library [111]. The convergence of the adjustment procedure has been achieved in three iterations. In the case of the full data set (346 cross sections) 222 data points survive rejection criterion and give an identical result to the one published earlier [21] on the evaporation-residue cross sections normalized with the σ_{reac} due to Shen [105]. It was stated already that we are interested in the data of fusion region III. Thus, in contrast to Ref. [21] the fitting is restricted to 256 data points, satisfying the condition $E_{\text{c.m.}}/A_{\text{tot}} > 1.0$ MeV/nucleon because, as is shown later, the transition from fusion region II to region III occurs at $E_{\text{c.m.}}/A_{\text{tot}} = 1.058 \pm 0.055$ MeV/nucleon. The fitting procedure stops in four iterations, and 178 data points surviving the rejection criterion are displayed in Fig. 8. The distribution of errors of all normalized fusion data of Table I is displayed by a histogram (inset in Fig. 8).

The obtained fit is rather stable with small uncertainty on the fit parameters (see the narrow orange band around the best-fit curve in Fig. 8). One infers from it and from Table IV that the fusion process is extinct at the (system) available energy $E_{\text{c.m.}}/A_{\text{tot}} = 13.3 \pm 0.9$ MeV/nucleon.²

²When no energy cut is applied to the data the energy of fusion disappearance is at $E_{\text{c.m.}}/A_{\text{tot}} = 13.2 \pm 0.5$ MeV/nucleon. Strictly the same result is obtained when Shen's value [105] instead of Tripathi's value [24] for σ_{reac} is taken for the σ_{fus} normalization and

B. Evaporation residue data

As it was stated above, we focus on incident energies several times higher than the fusion barrier. At these energies a formed compound nucleus may decay not only by evaporation, giving rise to an evaporation residue, but also via fissioning. In the experimental extraction of σ_{fus} values at these energies the main difficulty is in disentangling the contribution of a genuine fusion process from the competing reaction mechanisms, chiefly from damped collisions which lead to a fission without the formation of a compound nucleus [114,115]. Such a scenario is highly probable for heavier systems although the mass asymmetry plays a certain role too. Even with a high-performance detection apparatus it is sometimes impossible to distinguish fragments arising from these two reaction mechanisms. For instance, fragments of a fusion-fission process subjected to a small momentum transfer may be contaminated by the targetlike fragments of damped reactions being exposed to a similar momentum transfer.

By restricting the analysis to the experiments claiming the absence of fission in their yields, the cross-section data drops from 382 to 274 or to 238 out of 346 data values listed in columns 5 and 7 of Table I and shown in previous figures. The difference between these numbers comes from the 36 CF data points of column 6 of Table I. These fusion-evaporation points of Fig. 7 are displayed in Fig. 9. The existence of the arclike structure in the fusion-evaporation data in the σ_{fus}^N vs $E_{\text{c.m.}}/A_{\text{tot}}$ representation is now rendered irrefutable with a mere handful of points outside the global data trend. The number of fusion-evaporation points belonging to the fusion region III, i.e., with $E_{\text{c.m.}}/A_{\text{tot}} > 1.0$ MeV/nucleon is 181.

The above fitting strategy applied to this set of evaporation-residue data with the same probe function (4) gives almost exactly the same result as the fit over the full fusion-data set. This may be inferred from the values of the fit coefficients of the corresponding rows in Table IV: The best fit curve of Fig. 8 (thin dashed black curve in Fig. 9) is almost identical to the one fitting the evaporation-residue data (full thick red curve in Fig. 9). The uncertainty on fitting coefficients is slightly higher (see the orange band around the best fit curve in Fig. 9) so that the predicted energy for the fusion extinction is $E_{\text{c.m.}}/A_{\text{tot}} = 13.35 \pm 0.75$ MeV/nucleon.³

C. Complete fusion data

Among the experiments listed in our systematics only 12 have explicitly been designed to measure both complete and incomplete fusion components (see the CF column of Table I).

the same within the stated error in the case of a normalization using the σ_{reac} due to Kox [104].

³A fit without restricting the data to the fusion region III gives $E_{\text{c.m.}}/A_{\text{tot}} = 13.2 \pm 0.7$ MeV/nucleon. A fit to the same data using the Shen [105] formula for σ_{reac} for the normalization purpose results in fusion disappearance at $E_{\text{c.m.}}/A_{\text{tot}} = 13.2 \pm 0.6$ MeV/nucleon [21]. The values of thus deduced fit parameters may be found in Table I of Ref. [21].

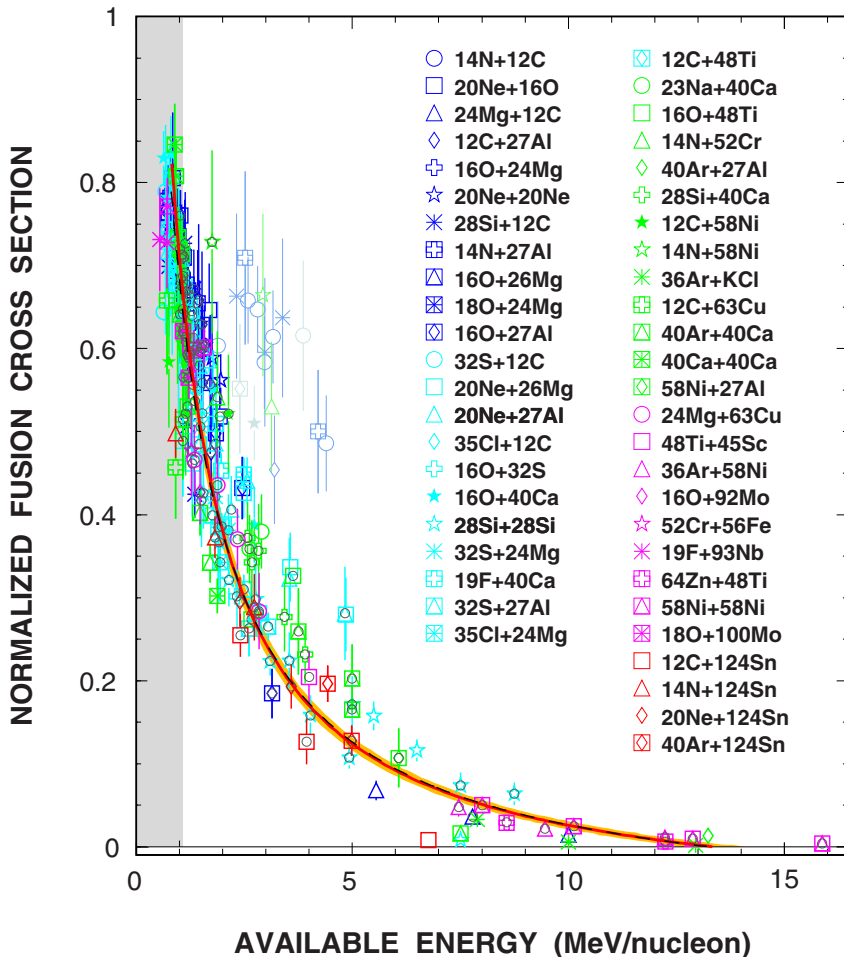


FIG. 9. (Color online) σ_{fus}^N yields as a function of $E_{\text{c.m.}}/A_{\text{tot}}$ of those fusion experiments in which no fission contribution has been reported. These 48 reactions and 238 data points are labeled by the same symbols and levels of gray (colors online) as in Fig. 1. Data points of the group ① in Fig. 7 are drawn by thinner lines and lighter colors. The full (red) curve is due to the best fit with the homographic function (4) to the subset of 181 evaporation-residue data points satisfying the condition $E_{\text{c.m.}}/A_{\text{tot}} > 1.0$ MeV/nucleon, i.e., to the points lying outside the light-gray band. (For the explanation of the light-gray band, see the caption to Fig. 7 and the text.) The thin dashed black curve is the same kind of fit to the full set of CF + IF data fulfilling the above energy requirement, i.e., the fit curve of Fig. 8. Those 126 data points which survived the rejection through the iterative fitting procedure are made visible by thin dark gray circles drawn over them.

This allows establishing a complete fusion (CF) excitation function which incorporates 60 σ_{fus} data points relative to 14 systems spanning a total mass range from 40 to 68 and average $\langle \mu \rangle$ and $\langle N_{\text{tot}}/Z_{\text{tot}} \rangle$ of 0.256 and 1.021, respectively. These data are plotted in Fig. 10. Inset in Fig. 10 displays the above 60 σ_{fus}^N values vs the inverse of the available energy $1/(E_{\text{c.m.}}/A_{\text{tot}})$. Expressing abscissas in units of the inverse of the center-of-mass energy $1/E_{\text{c.m.}}$ is a very popular presentation of (complete) fusion data because it nicely emphasizes the three fusion regions discussed in Sec. I: the rising (region I), stagnating (region II), and falling (region III) feature of σ_{fus} as energy increases from the reaction threshold (see, e.g., in Refs. [3,17]). As was mentioned in Sec. I and owing to the relation (2) in the σ_{fus} vs $1/E_{\text{c.m.}}$ presentation the fusion excitation function is in each of regions depicted by a segment of a straight line. The inset in Fig. 10 generalizes such a presentation to scaled σ_{fus}^N and to the inverse of $E_{\text{c.m.}}/A_{\text{tot}}$. This generalization brings different systems to lie over each other on common curves—segments of homographic functions—and not on straight lines. The second, stagnating and the third, falling regions of fusion are clearly distinguished. The same fitting strategy with the homographic probe function (4) was applied to each of the two fusion regions. The fit over the 10 CF points of region II is obtained in a single iteration. It is represented by a (dark green) dash-dotted curve which is close to a horizontal line. A fit over the remaining 50 CF

points of region III was achieved in two iterations leaving 47 data points; see the fit parameters in Table IV and a (violet) full curve in both the inset and the main panel in Fig. 10. The break of the slope delimiting the fusion regions II and III occurs at $E_{\text{c.m.}}/A_{\text{tot}} = 1.06 \pm 0.06$ MeV/nucleon independently of the system studied. The uncertainty on regions II and III limiting energy is inferred from the errors attributed to the fit parameters, which are represented by the (light-violet) zone around the fit curve. The falling branch of the fusion region III at $1/(E_{\text{c.m.}}/A_{\text{tot}}) < 0.945 \pm 0.050$, i.e., the CF data for $E_{\text{c.m.}}/A_{\text{tot}} > 1.06 \pm 0.06$ MeV/nucleon, is the portion of the data relevant to the fusion disappearance and is our particular interest. This fact is emphasized in Figs. 7–9 by the light-gray zone.

In the main panel in Fig. 10 are plotted only the 50 CF points belonging to the region III of fusion. Data of the same experiments discussed in the case of incomplete fusion results belonging to group ① in Fig. 7, namely 3 points of the $^{28}\text{Si} + ^{12}\text{C}$ [31] and a single data point of the $^{32}\text{S} + ^{12}\text{C}$ reaction [41], are again outside the general data trend. Thus, they are labeled by lighter colors of the symbols. The best-fit homographic function decreases rapidly as a function of $E_{\text{c.m.}}/A_{\text{tot}}$ and crosses the abscissa axis at around 6 MeV/nucleon. In contrast to the fit of the global fusion data errors on the fit parameters are now much larger and one may infer that the complete fusion reaction process disappears at

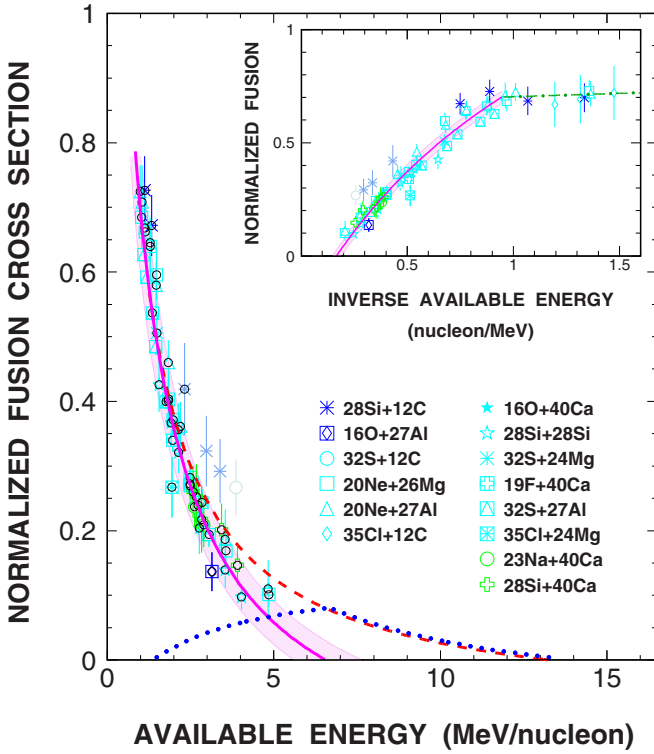


FIG. 10. (Color online) Normalized complete fusion cross section σ_{fus}^N as a function of $E_{\text{c.m.}}/A_{\text{tot}}$ (main panel) and as a function of the inverse of the same energy (inset) from those measurements which have reported data on both complete and incomplete fusion. The full (violet) curve in the inset and the main panel is due to the best fit of the complete fusion data by the homographic function (4) in the falling (third) region of fusion cross section. The (dark green) dash-dotted curve in inset is due to the same kind of fit to the stagnating (second) region of fusion cross section. The background band around the best fit curve in the main panel and in the inset is due to the errors on the fit parameters provided by the code used [111]. The (red) dashed curve is from Fig. 8 and it represents the best-fit homographic function of the normalized fusion cross sections of Fig. 7. The (blue) dotted curve is the difference of both. Those data points which survived the rejection through the iterative fitting procedure are made visible by the thin dark-gray circles drawn over them.

$E_{\text{c.m.}}/A_{\text{tot}} = 6.6 \pm 1.0$ MeV/nucleon.⁴ For the CF reaction mechanism, the center-of-mass energy and the excitation energy are equivalent. Thus, the energy limit of about 6.5 ± 1.0 MeV/nucleon corresponds to the maximal excitation energy which can be deposited into such a light compound nucleus decaying by evaporation. The question is whether the observed functional dependence and extinction energy remain unchanged for heavier and more mass asymmetric systems. Clearly, more σ_{fus} data are needed.

⁴Fit curves without restriction to fusion region III give for the energy of complete fusion disappearance $E_{\text{c.m.}}/A_{\text{tot}} = 6.2_{-1.0}^{+1.3}$ MeV/nucleon, whereas under the same conditions for cut in energy but for evaporation residue data [21] a normalization by the Shen formula [105] gives exactly the same result with a slight difference on the lower uncertainty: $E_{\text{c.m.}}/A_{\text{tot}} = 6.2_{-1.1}^{+1.3}$ MeV/nucleon.

V. DISCUSSION AND SUMMARY

In this work we report on the excitation function of the published fusion cross section at incident energies higher than about $3A - 4A$ MeV. This scrutiny resulted in 382 fusion-evaporation and/or fusion-fission cross-section data points belonging to 81 different systems from works published between 1972 and 2011. The accumulated data span over a large range in system mass, mass asymmetry, and neutron-to-proton content. In these four decades experimental techniques and related uncertainties in data collection have evolved considerably from (i) use of mica for charged particle tracking over (ii) coincident $\Delta E - E$ telescope technique for detecting charge of reaction products, (iii) time-of-flight approach providing mass of reaction products, and/or (iv) in-beam γ -spectroscopy technique allowing identification of non-ground-state reaction products to (v) modern multidetector arrays providing event-by-event reconstruction of charged reaction products. In spite of the unequal accuracy of existing fusion data, our analysis allowed deeper insight into the evolution of the underlying reaction mechanisms as a function of entrance channel parameters. Normalized by the reaction cross section and plotted as a function of center-of-mass energy per nucleon, the fusion cross section allows us to draw a rather universal homographic law for its dependence on energy. The universal feature of thus scaled fusion data becomes especially clear when one ignores the experimental data of the somewhat more uncertain fission-to-fusion contribution. The fusion data restricted to the evaporation-residue contribution do not alter, however, the parameters of the best-fit homographic function.

The dashed (red) curve in Fig. 10 is in fact the best-fit function from Fig. 8. It represents the sum of the CF and incomplete fusion (IF) components for the scaled-axes presentation of the fusion region III data, i.e., of those $\sigma_{\text{fus}}/\sigma_{\text{reac}}^T$ points (column 7 of Table I) for which the corresponding energy $E_{\text{c.m.}}/A_{\text{tot}}$ (column 4 of Table I) is larger than 1.0 MeV/nucleon. Dissociating the complete and incomplete fusion cross sections allows us to provide fairly accurate energy limits characterizing these two mechanisms. Indeed, the CF and CF + IF fusion excitation functions impart that the complete fusion reaction mechanism disappears at $E_{\text{c.m.}}/A_{\text{tot}} = 6.6 \pm 1.0$ MeV/nucleon, whereas the incomplete fusion vanishes at $E_{\text{c.m.}}/A_{\text{tot}} = 13.3 \pm 0.9$ MeV/nucleon. For mass symmetric systems the above values convert into incident energy of about $26A$ and $53A$ MeV, respectively. The difference of the dashed CF + IF fit curve and the full CF fit curve allows us to infer the excitation function of the IF component, shown in Fig. 10 by the dotted curve. These curves provide a measure of the average contribution of the CF and IF components in (total) reaction cross section and of their evolution with the system available energy $E_{\text{c.m.}}/A_{\text{tot}}$.

From these results one can, in particular, conclude the following:

- (i) The threshold of IF is around $E_{\text{c.m.}}/A_{\text{tot}} \approx 1.5$ MeV/nucleon.
- (ii) The CF decreases while the IF increases. Both components contribute about the same at $E_{\text{c.m.}}/A_{\text{tot}} \approx 5$ MeV/nucleon and each represent about 7% of σ_{reac} .

- (iii) The IF component increases up to 6.5 MeV/nucleon, where it reaches a maximum corresponding to about 8% of σ_{reac} while at the same time the CF process vanishes.
- (iv) The IF component then decreases and disappears around $E_{\text{c.m.}}/A_{\text{tot}} = 13$ MeV/nucleon.

To the best of our knowledge, this is the first time that accurate limits concerning both fusion components have been extracted from a such large body of data. It allows us to draw a simple picture for the evolution of these reaction mechanisms. This result is pertinent for constraining parameters of models used to simulate nuclear reactions, in particular those meant to encompass in a single code a variety of reaction mechanisms at intermediate energies such as the code HIPSE [116].

The recent experimental evidence of an unexpectedly weakened nuclear stopping power around the Fermi energy [117], which corroborates earlier theoretical predictions of a nuclear pseudotransparency of heavy-ion reactions at the same energy range [118–120], puts forward a scenario where at these energies an interplay of a weakened nuclear mean field and a still insufficient stopping efficiency of nucleon-nucleon collisions is the cause of fusion disappearance [121]. Our recent simulations with the microscopic DYWAN semiclassical transport code [22], in contrast to other dynamical models [122,123], correctly describes the universality of IF excitation function in the energy range of the model applicability, i.e., above $\gtrsim 15$ A MeV [21]. Moreover, these simulations strongly corroborate that the lack of nuclear stopping power is at the origin of the fusion disappearance.

Let us finally remind that a single measurement has been carried out at incident energies higher than 100A MeV [89]. The authors report that (incomplete) fusion of heavy asymmetric systems persists and tends towards a constant value as energy increases. We have explained these observed cross sections within a semiclassical microscopic theory and the asymptotic behavior of these data by a simple estimate using the reaction geometry [110]. Both performed calculations call for the participant-spectator-like picture [112] as the underlying reaction mechanism. It would be of obvious interest to experimentally measure fusion in the energy gap of missing data, namely, between 35A MeV and 100A MeV, to nail down

the evolution of heavy-ion reaction mechanism from fusion to the one dominated by reaction geometry.

To summarize, the systematics and analysis of fusion cross section data above the reaction threshold region allowed us to infer the following:

- (1) A universal homographic law derived from the basic nuclear reaction formula describing fusion excitation functions. It does not depend on the characteristics of the reaction system—its size, mass asymmetry, and isospin. Such a result may be used as a stringent test for reaction models.
- (2) The same functional dependence is valid for complete (CF) and incomplete (IF) evaporation fusion data.
- (3) The main characteristics of IF reaction mechanism are determined—its threshold, maximum, and disappearance energies.
- (4) Exactly the same functional dependence has been found when IF data of fusion-fission component are added to IF-evaporation data, although the correlation is somewhat weaker, which may be explained by the larger experimental uncertainties and by a possible influence of normalization.
- (5) A corollary of the universality of the deduced excitation functions is the identification of those experimental data which are the most likely suffering from the unusually large systematic errors.
- (6) Data obtained at incident energies higher than 100A MeV and which are out of the universal law for fusion excitation function have been conveniently explained.
- (7) Moreover, this comprehensive analysis allowed us to identify incident-energy vs reaction-system characteristics which are modestly covered or uncovered by the existing fusion data. We urge for additional measurements.

ACKNOWLEDGMENT

Z.B. gratefully acknowledges the financial support and the hospitality of the Faculté des Sciences et Techniques, University of Nantes and the Laboratory SUBATECH, UMR 6457. This work has been supported in part by Croatian Science Foundation under the Project No. 7194.

-
- [1] R. Bass, *Nucl. Phys. A* **231**, 45 (1974).
 - [2] J. R. Birkelund *et al.*, *Phys. Rep.* **56**, 107 (1979).
 - [3] R. Bass, *Nuclear Reactions with Heavy Ions* (Springer, Berlin, 1980).
 - [4] W. J. Swiatecki, *Nucl. Phys. A* **376**, 275 (1982).
 - [5] J. R. Birkelund and J. R. Huizinga, *Ann. Rev. Nucl. Part. Sci.* **33**, 265 (1983).
 - [6] P. Fröbrich, *Phys. Rep.* **116**, 337 (1984).
 - [7] R. J. Charity *et al.*, *Nucl. Phys. A* **457**, 441 (1986).
 - [8] P. Fröbrich and I. I. Gontchar, *Phys. Rep.* **292**, 131 (1998).
 - [9] R. Giordano *et al.*, *Nuovo Cimento A* **103**, 47 (1990).
 - [10] M. Dasgupta *et al.*, *Ann. Rev. Nucl. Part. Sci.* **48**, 401 (1998), and references therein.
 - [11] http://flerovlab.jinr.ru/flnr/knowledge_base.html, and references therein.
 - [12] L. F. Canto *et al.*, *Phys. Rep.* **424**, 1 (2006).
 - [13] B. B. Back, H. Esbensen, C. L. Jiang, and K. E. Rehm, *Rev. Mod. Phys.* **86**, 317 (2014).
 - [14] H. Morgenstern, W. Bohne, W. Galster, K. Grabisch, and A. Kyanowski, *Phys. Rev. Lett.* **52**, 1104 (1984).
 - [15] P. Lautesse *et al.*, *Eur. Phys. J. A* **27**, 349 (2006).
 - [16] D. G. Kovar *et al.*, *Phys. Rev. C* **20**, 1305 (1979).
 - [17] U. Mosel, in *Treatise on Heavy-Ion Science*, edited by D. A. Bromley (Plenum Press, New York, 1984), Vol. 2, p. 3.
 - [18] H. Esbensen, *Phys. Rev. C* **85**, 064611 (2012).
 - [19] P. Eudes *et al.*, in *Proceedings of the 11th International Conference on Nucleus-Nucleus Collisions*, edited by B.-A. Li and J. Natowitz, *J. Phys.: Conf. Series* 420 (IOP, London, 2013).

- [20] P. Eudes *et al.*, in *Proceedings of the IWM2011 International Workshop on Multifragmentation and Related Topics*, edited by J. D. Frankland, A. Pagano, S. Pirrone, M.-F. Rivet, and F. Rizzo (Italian Physical Society, Bologna, 2012), p. 181.
- [21] P. Eudes *et al.*, *Europhys. Lett.* **104**, 22001 (2013).
- [22] B. Jouault *et al.*, *Nucl. Phys. A* **628**, 119 (1998); V. de la Mota and F. Sébille, *Eur. Phys. J. A* **12**, 479 (2001); F. Sébille, V. de la Mota, I. C. Sagrado Garcia, J. F. Lecolley, and V. Blideanu, *Phys. Rev. C* **76**, 024603 (2007).
- [23] M. Lefort, *J. Phys. A: Math. Nucl. Gen.* **7**, 107 (1974); *Rep. Prog. Phys.* **39**, 129 (1976).
- [24] R. K. Tripathi, F. A. Cucinotta, and J. W. Wilson, *Nucl. Instr. Meth. Phys. Res. B* **117**, 347 (1996).
- [25] J. Gomez del Campo, R. G. Stokstad, J. A. Biggerstaff, R. A. Dayras, A. H. Snell, and P. H. Stelson, *Phys. Rev. C* **19**, 2170 (1979).
- [26] R. G. Stokstad *et al.*, *Phys. Lett. B* **70**, 289 (1977).
- [27] D. Shapira *et al.*, *Phys. Rev. C* **28**, 1148 (1983).
- [28] M. Samri *et al.*, *Phys. Rev. C* **65**, 061603(R) (2002).
- [29] J. B. Natowitz, E. T. Chulick, and M. N. Namboodiri, *Phys. Rev. C* **6**, 2133 (1972).
- [30] S. L. Tabor, D. F. Geesaman, W. Henning, D. G. Kovar, K. E. Rehm, and F. W. Prosser, *Phys. Rev. C* **17**, 2136 (1978).
- [31] M. F. Vineyard *et al.*, *Phys. Rev. C* **47**, 2374 (1993).
- [32] B. A. Harmon, S. T. Thornton, D. Shapira, J. Gomez del Campo, and M. Beckerman, *Phys. Rev. C* **34**, 552 (1986).
- [33] M. N. Namboodiri, E. T. Chulick, J. B. Natowitz, and R. A. Kenefick, *Phys. Rev. C* **11**, 401 (1975).
- [34] B. B. Back *et al.*, *Nucl. Phys. A* **285**, 317 (1977).
- [35] R. L. Kozub *et al.*, *Phys. Rev. C* **11**, 1497 (1975).
- [36] G. P. Gilfoyle *et al.*, *Phys. Rev. C* **46**, 265 (1992).
- [37] J. J. Kolata, R. A. Racca, P. A. DeYoung, E. Aguilera-Reyes, and M. A. Xapsos, *Phys. Rev. C* **32**, 1080 (1985).
- [38] N. Arena *et al.*, *Nuovo Cimento A* **100**, 953 (1988).
- [39] N. Arena, S. Cavallaro, S. Femino, P. Figuera, S. Pirrone, F. Porto, and S. Sambataro, *Phys. Rev. C* **44**, 1947 (1991).
- [40] R. Giordano *et al.*, *Nuovo Cimento A* **77**, 135 (1983).
- [41] S. Pirrone *et al.*, *Phys. Rev. C* **64**, 024610 (2001).
- [42] H. Lehr *et al.*, *Nucl. Phys. A* **415**, 149 (1984).
- [43] H. Morgenstern *et al.*, *Z. Phys. A* **313**, 39 (1983).
- [44] S. Pirrone *et al.*, *Phys. Rev. C* **55**, 2482 (1997).
- [45] C. Beck *et al.*, *Z. Phys. A* **343**, 309 (1992).
- [46] C. Beck *et al.*, *Phys. Rev. C* **54**, 227 (1996).
- [47] S. E. Vigdor, D. G. Kovar, P. Sperr, J. Mahoney, A. Menchaca-Rocha, C. Olmer, and M. S. Zisman, *Phys. Rev. C* **20**, 2147 (1979).
- [48] C. Beck *et al.*, *Phys. Rev. C* **39**, 2202 (1989).
- [49] S. B. DiCenzo, J. F. Petersen, and R. R. Betts, *Phys. Rev. C* **23**, 2561 (1981).
- [50] M. F. Vineyard *et al.*, *Phys. Rev. C* **41**, 1005 (1990).
- [51] R. J. Meijer *et al.*, *Phys. Rev. C* **44**, 2625 (1991).
- [52] A. Oberstedt *et al.*, *Nucl. Phys. A* **548**, 525 (1992).
- [53] P. F. Box *et al.*, *Phys. Rev. C* **50**, 934 (1994).
- [54] D. G. Kovar *et al.*, *Bull. Am. Phys. Soc.* **22**, 66 (1977).
- [55] J. D. Hinnefeld *et al.*, *Phys. Rev. C* **36**, 989 (1987).
- [56] G. Rosner *et al.*, *Phys. Lett. B* **150**, 87 (1985).
- [57] J. Pochodzalla *et al.*, *Phys. Lett. B* **181**, 33 (1986).
- [58] C. Beck *et al.*, *Eur. Phys. J. A* **2**, 281 (1998).
- [59] S. Cavallaro *et al.*, *Phys. Rev. C* **57**, 731 (1998).
- [60] P. L. Gonthier *et al.*, *Nucl. Phys. A* **411**, 289 (1983).
- [61] J. Péter *et al.*, *Nucl. Phys. A* **593**, 95 (1995).
- [62] M. F. Vineyard *et al.*, *Phys. Rev. C* **45**, 1784 (1992).
- [63] E. Bisquer, Ph.D. thesis, Université Claude Bernard, Lyon I, 1996 (unpublished).
- [64] J. Carter *et al.*, *Z. Phys. A* **313**, 57 (1983).
- [65] W. Rösch *et al.*, *Phys. Lett. B* **197**, 19 (1987).
- [66] W. Rösch *et al.*, *Nucl. Phys. A* **496**, 141 (1989).
- [67] R. Gentner *et al.*, *Z. Phys. A* **347**, 117 (1993).
- [68] H. Doubre *et al.*, *Phys. Lett. B* **73**, 135 (1978).
- [69] L. Lebreton *et al.*, *Eur. Phys. J. A* **3**, 325 (1998).
- [70] B. Borderie *et al.*, *Z. Phys. A* **298**, 235 (1980).
- [71] H. Stege *et al.*, *Nucl. Phys. A* **489**, 146 (1988).
- [72] S. Agarwal *et al.*, *Z. Phys. A* **296**, 287 (1980).
- [73] G. Guillaume *et al.*, *Phys. Rev. C* **26**, 2458 (1982).
- [74] A. Fahli *et al.*, *Phys. Rev. C* **34**, 161 (1986).
- [75] B. John, S. K. Kataria, B. S. Tomar, A. Goswami, G. K. Gubbi, and S. B. Manohar, *Phys. Rev. C* **56**, 2582 (1997).
- [76] M. P. Kelly, J. F. Liang, A. A. Sonzogni, K. A. Snover, J. P. S. van Schagen, and J. P. Lestone, *Phys. Rev. C* **56**, 3201 (1997).
- [77] G. Ademard *et al.*, *Phys. Rev. C* **83**, 054619 (2011).
- [78] H. Nifenecker *et al.*, *Nucl. Phys. A* **447**, 533 (1986).
- [79] J. Blachot *et al.*, *Z. Phys. A* **303**, 85 (1981).
- [80] H. C. Britt *et al.*, *Phys. Rev. C* **13**, 1483 (1976).
- [81] M. Lefort, *Phys. Rev. C* **12**, 686 (1975).
- [82] L. C. Vaz *et al.*, *Z. Phys. A* **311**, 89 (1983).
- [83] B. Borderie *et al.*, *Z. Phys. A* **316**, 243 (1984).
- [84] D. Logan *et al.*, *Phys. Rev. C* **22**, 1080 (1980).
- [85] B. Tamain, C. Ngô, J. Péter, and F. Hanappe, *Nucl. Phys. A* **252**, 187 (1975).
- [86] H. Oeschler *et al.*, *Phys. Lett. B* **127**, 177 (1983).
- [87] H. Oeschler, H. Freiesleben, K. D. Hildenbrand, P. Engelstein, J. P. Coffin, B. Heusch, and P. Wagner, *Phys. Rev. C* **22**, 546 (1980).
- [88] D. Prindle *et al.*, *Phys. Rev. C* **57**, 1305 (1998).
- [89] A. A. Sonzogni *et al.*, *Phys. Rev. C* **53**, 243 (1996).
- [90] J. D. Hinnefeld *et al.*, *Phys. Lett. B* **225**, 308 (1989).
- [91] D. Prindle, R. Vandebosch, S. Kailas, A. Charlop, and C. Hyde-Wright, *Phys. Rev. C* **48**, 291 (1993).
- [92] J. Cabrera *et al.*, *Phys. Rev. C* **68**, 034613 (2003).
- [93] F. L. H. Wolfs *et al.*, *Phys. Lett. B* **196**, 113 (1987).
- [94] D. Hilscher *et al.*, *Phys. Rev. C* **36**, 208 (1987).
- [95] J. M. Miller *et al.*, *Phys. Rev. Lett.* **40**, 1074 (1978).
- [96] B. Borderie *et al.*, *Z. Phys. A* **299**, 263 (1981).
- [97] H. A. Khan, T. Lund, P. Vater, R. Brandt, and J. W. N. Tuyn, *Phys. Rev. C* **28**, 1630 (1983).
- [98] C. Egelhaaf *et al.*, *Nucl. Phys. A* **405**, 397 (1983).
- [99] G. La Rana *et al.*, *Nucl. Phys. A* **407**, 233 (1983).
- [100] C. Ngô, J. Péter, B. Tamain, M. Berlanger, and F. Hanappe, *Z. Phys. A* **283**, 161 (1977).
- [101] E. Duek *et al.*, *Z. Phys. A* **307**, 237 (1982).
- [102] H. K. W. Leege *et al.*, *Phys. Rev. C* **46**, 991 (1992).
- [103] M. Kildir *et al.*, *Z. Phys. A* **306**, 323 (1982).
- [104] S. Kox *et al.*, *Phys. Rev. C* **35**, 1678 (1987).
- [105] W. Shen, B. Wang, J. Feng, W.-I. Zhan, Y. Zhu, and E. Feng, *Nucl. Phys. A* **491**, 130 (1989).
- [106] L. Sihver, C. H. Tsao, R. Silberberg, T. Kanai, and A. F. Barghouty, *Phys. Rev. C* **47**, 1225 (1993).
- [107] P. Shukla, *Phys. Rev. C* **67**, 054607 (2003).
- [108] B. Abu-Ibrahim, *Phys. Rev. C* **83**, 044615 (2011).
- [109] I. Angelis, *At. Data Nucl. Data Tables* **87**, 185 (2004).
- [110] P. Eudes *et al.*, *Nucl. Phys. A* (2014), doi:10.1016/j.nuclphysa.2014.07.035.

- [111] F. James and M. Roos, *Comput. Phys. Commun.* **10**, 343 (1975).
- [112] G. D. Westfall *et al.*, *Phys. Rev. Lett.* **37**, 1202 (1976).
- [113] T. Matsuse, A. Arima, and S. M. Lee, *Phys. Rev. C* **26**, 2338 (1982).
- [114] H. Fuchs and K. Möhring, *Rep. Prog. Phys.* **57**, 231 (1994).
- [115] C.-K. Gelbke and D. H. Boal, *Prog. Part. Nucl. Phys.* **19**, 33 (1987).
- [116] D. Lacroix, A. Van Lauwe, and D. Durand, *Phys. Rev. C* **69**, 054604 (2004).
- [117] G. Lehaut *et al.* (INDRA Collaboration), *Phys. Rev. Lett.* **104**, 232701 (2010).
- [118] P. Eudes, Z. Basrak, and F. Sébille, *Phys. Rev. C* **56**, 2003 (1997).
- [119] I. Novosel *et al.*, *Phys. Lett. B* **625**, 26 (2005).
- [120] Z. Basrak, *Nucl. Phys. A* **738**, 463 (2004).
- [121] Z. Basrak and P. Eudes, in *Proceedings of the International Conference on Clustering Aspects of Nuclear Structure and Dynamics*, edited by M. Korolija, Z. Basrak, and R. Čaplar (World Scientific, Singapore, 2000), p. 316.
- [122] H. M. Xu, W. G. Lynch, P. Danielewicz, and G. F. Bertsch, *Phys. Rev. Lett.* **65**, 843 (1990); *Nucl. Phys. A* **568**, 365 (1994).
- [123] L. Shvedov, M. Colonna, and M. Di Toro, *Phys. Rev. C* **81**, 054605 (2010).